LA-3754

63

LOS ALAMOS SCIENTIFIC LABORATORY
of the
University of California
LOS ALAMOS • NEW MEXICO

The 1965 ARPA-AEC Joint Lightning Study at Los Alamos

Volume I

UNITED STATES
ATOMIC ENERGY COMMISSION
CONTRACT W-7405-ENG. 36

LEGAL NOTICE

This report expresses the opinions of the author or authors and does not necessarily reflect the opinions or views of the Los Alamos Scientific Laboratory.

Printed in the United States of America. Available from
Clearinghouse for Federal Scientific and Technical Information
National Bureau of Standards, U. S. Department of Commerce
Springfield, Virginia 22151
Price: Printed Copy $3.00; Microfiche $0.65

BLANK PAGE

LA-3754
UC-34, PHYSICS
TID-4500

LOS ALAMOS SCIENTIFIC LABORATORY
of the
University of California
LOS ALAMOS • NEW MEXICO

Report written: May 1967

Report distributed: December 5, 1967

The 1965 ARPA-AEC Joint Lightning Study at Los Alamos*

Volume I

The Lightning Spectrum. Charge Transfer in Lightning. Efficiency of Conversion of Electrical Energy into Visible Radiation.

by

T. Robert Connor

*Work done under the auspices of the AEC in response to ARPA Order No. 631, Program Code No. 5820

CONTENTS

VOLUME I*

* Other volumes covering different aspects of the 1965 ARPA-AEC Joint Lightning Study at Los Alamos are:

LA-3755	Volume II.	Comparison of the Lightning Spectrum with Narrow-Field and All-Sky Photometer Data
LA-3756	Volume III.	Propagation of Light into All-Sky Detectors
LA-3757	Volume IV.	Discrimination and False Alarm Analysis

THE 1965 ARPA-AEC JOINT LIGHTNING STUDY AT LOS ALAMOS

VOLUME I

THE LIGHTNING SPECTRUM. CHARGE TRANSFER IN LIGHTNING. EFFICIENCY OF CONVERSION OF ELECTRICAL ENERGY INTO VISIBLE RADIATION

T. Robert Connor

ABSTRACT

In the summer of 1965 the Atomic Energy Commission and the Department of Defense (ARPA) sponsored studies of the optical and electromagnetic emissions of lightning at Los Alamos, N. M., to obtain information for improving lightning discrimination methods in high altitude air fluorescence detection systems. The project was a coordinated effort among LASL, EG&G, DRI, and a small AWRE team. LASL obtained slitless spectra of 11 strokes from six flashes. The analysis and evaluation of these spectra and correlated electric field data are the subject of this report.

The spectra were of the following types: (1) ten stroke-resolved spectra of first and subsequent return strokes, (2) time-resolved spectra of two continuing luminosities, (3) the spectrum at three different heights along the channel of a single return stroke. All are fully reduced in terms of flux (erg/Å-cm^2) at the entrance pupil of the spectrograph and corrected for atmospheric transmission. While not a large statistical sample, these spectra are of considerable value, for they are the only quantitatively reduced spectra covering the full visible wavelength range.

The spectrum of lightning consists of a strong continuum with strong lines attributable to NII, NI, HI, and OI. The spectra of first return strokes differ from those of subsequent return strokes and continuing luminosities. If the best straight-line fit is made to the continuum, the ratios of continuum in the vicinity of 3900 Å to that in the vicinity of 6900 Å are 2.0, 1.6, and 1.0 for first return strokes, subsequent return strokes, and continuing luminosities, respectively. These ratios indicate decreasing channel temperatures in the order given. Also, if the ratio of NII radiation to NI radiation is used as a measure of excitation and ionization, then first return strokes have the highest degree of excitation and ionization of the three lightning phenomena, and continuing luminosities have the lowest.

On the basis of the 10 return-stroke spectra, considering atmospheric transmission and photodetector sensitivities, the blend of NII multiplets at 5000 Å and the Hα line at 6563 Å appear to be the most outstanding

features with a potential for discrimination applications. Under a variety of storm and background light conditions, the 5000-Å feature may be even better than the 6563-Å line.

The charge transferred to ground and the energy deposited in the channel were calculated using electromagnetic data and photographic ranging data. Using data on 18 strokes from six flashes, averages of charge transferred to ground are 7 coulombs/stroke, and 28 coulombs/flash. The energy per meter of channel deposited by a return stroke ranged between 2×10^4 and 3×10^5 joules/meter. The efficiency for the conversion of electrical energy to visible (3900- to 6900-Å) radiation was calculated to be 0.7%.

I. INTRODUCTION

During the 1965 ARPA-AEC joint lightning study at Los Alamos, coordinated data were obtained from a time-resolved spectrograph, from collimated photometers with narrow spectral bandpasses, from all-sky photometers similar to those used in the LASL High Altitude Air Fluorescence Detection System, and from antennas designed to study the electromagnetic emissions produced by lightning. The study was undertaken to obtain basic data on the physics of lightning and statistical information on its optical and electromagnetic emissions to improve lightning discrimination methods in Vela Sierra systems. The results of the spectrographic and LASL electromagnetic-pulse studies are discussed and applied to the problem of discrimination.

The literature on the optical spectrum of lightning from 1901 to 1960[1] shows that the spectra obtained by different techniques differ significantly in certain features of importance to designers of systems intended to detect high altitude air fluorescence from clandestine nuclear tests in space. Those investigators, including Salanave, who employed slitless spectrographs, report a strong continuum throughout the visible wavelength range with strong line features from neutral and singly ionized atoms, in some cases with a wide water-vapor absorption band extending from 5900 to 6000 Å, and in a few (approximately 5%) cases with weak N_2^+ 1N molecular-band emission. On the other hand, those who employ conventional slit spectrographs to obtain long time exposures (1 to 2 hours) at night of all the light emitted by a lightning storm report that molecular bands in general, and the N_2^+ 1N bands in particular, are among the most dominant features in the visible spectrum. Since the detection of high altitude air fluorescence is based on a narrow optical bandwidth channel at the 3914-Å bandhead of the N_2^+ 1N (0,0) transition, it is important to obtain answers to the following questions: (1) What is the source of molecular-band radiation in a lightning storm? (2) Is this source capable of triggering the all-sky air fluorescence detection system? (3) If this source can trigger the all-sky detection system, can the system be modified to decrease the false alarm rate during lightning storms?

There are data in the literature which have a bearing on these questions. In 1903 Fox[2] observed, from slitless spectra, that relative intensities of various atomic line features in a lightning channel varied as a function of height along the channel. Then in 1941, Israel and Wurm,[3] using a slitless spectrograph, first made the now confirmed observation that the degree of ionization and excitation as measured by the ratio of radiation from singly ionized atoms to that from neutral atoms is highest near the bottom of the lightning channel and decreases toward the cloud. They also identified the N_2^+ 1N bands whose excitation followed that of the neutral atoms and was therefore a stronger spectral feature nearer the clouds.

Meinel and Salanave[4] have studied the possible source of N_2^+ emission in lightning storms and

limited the list of possibilities to the following:

(1) continuing luminosity in the main channel,

(2) the presumed fan of streamers within the cloud that spread the charge pulse,

(3) leader processes, or

(4) corona, which emanates from a large area of the earth's surface, and can produce long duration pulses with significant exposure in a time-integrated spectrum.

During the summer study, we obtained a number of time-resolved slitless spectra which were then fully reduced to give the incident, time-integrated, spectral flux (ergs/cm^{-2} Å^{-1}) at the entrance pupil of the spectrograph as a function of wavelength; these spectra were corrected for atmospheric transmission. In a search of the literature no other fully reduced spectra of lightning were found.

This report discusses these spectrographic data and the LASL electromagnetic pulse data in an attempt to answer some of the questions posed here and to extract a few more numbers to add to the meager supply of quantitative results on the physics of lightning.

II. SPECTROSCOPY OF LIGHTNING

A. Apparatus

The reduced spectra were obtained using the N4GS lens and grating slitless spectrograph[5] with film-aperture ratio of f/2.8 and dispersion of approximately 90 Å/mm. Figure 1 is a diagram of the N4GS optics. A measured resolution of about 6 Å was realized. Spectra covered the wavelength interval 3800 to 7000 Å. A horizontal slot at the normal slit plane defined the field of view to either 0.05° or 0.3° vertical by 16° horizontal (total angles). Time resolution, attained by film motion perpendicular to the direction of dispersion, was either 3 or 18 msec. The film used was Eastman Kodak 2475.

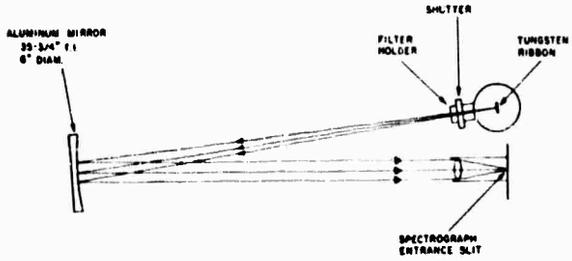

Fig. 2. Calibration setup for N4GS spectrograph.

B. Calibration

Figure 2 shows the setup of the calibration source. The tungsten ribbon was placed at the focus of the aluminum mirror, and the focus was checked with a theodolite. The image of the ribbon was then formed at the entrance slit by an objective lens and centered on the 100-μ-wide vertical slit used for calibration. The shutter open time was measured by placing a phototube inside the spectrograph at the plane A-A (Fig. 1) and displaying the signal on an

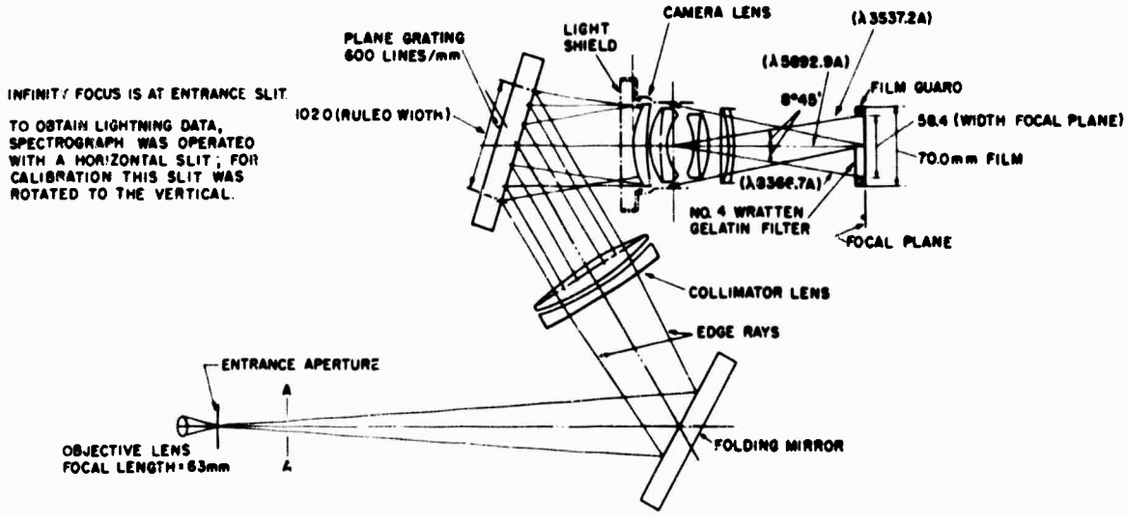

Fig. 1. Optics of the N4GS spectrograph.

oscilloscope. Spectra of the tungsten filament were then recorded on film for various combinations of calibrated neutral density filters. A wavelength calibration was obtained by taking spectra of a mercury and a neon source. Sensitometric step wedges were impressed on the film which was then developed by a Versamat film processor.

The temperature of the tungsten filament was measured with a pyrometer and determined to be 2024.4°K. The brightness vs wavelength curve for the tungsten lamp was determined using W. Gould's RAY code.

A transmission, T(λ), was calculated at 100-Å intervals between 3800 and 7200 Å for each filter combination. This transmission is multiplied by the brightness, B(λ), of the tungsten lamp and by the exposure duration, τ, and divided by the product of dispersion, D, and the width, W, of the entrance slit in the film plane to give the time-integrated brightness, INTB(λ), of the image in the entrance slit,

$$INTB(\lambda) = [B(\lambda)\cdot T(\lambda)\cdot \tau]/D\cdot W \ \frac{ergs}{cm^2\cdot Å\cdot sr},$$

for an entrance-slit width corresponding to 1 Å in the film plane.

For the presentation of the data in final form, this brightness at the entrance slit is converted to flux at the entrance pupil.

C. Method of Data Reduction

The densitometry was carried out on the Eastman Kodak microdensitometer. The slit chosen was 25 μ high (the spectra ranged between 50 and 300 μ in height) and 150 μ wide (equivalent to 13.5 Å). Although the theoretical resolution of 3 Å for the spectrograph would have dictated the use of a slit approximately 30 μ wide, it was necessary to use the wider slit to lessen the noise in the densitometer tracing, since this noise was due to the graininess of the film. The densitometer was calibrated daily using a step wedge as a standard.

The densitometer tracings of the spectra were digitized and put on IBM cards, and the data reduction was carried out by a series of computer programs. A description of the data reduction of one of the spectra is given to illustrate the steps taken. The spectrum is that of a return stroke of flash number 103 of run 40 (hereafter referred to by Count No. 40.103), which was the stroke on which the photoelectric systems triggered. This was the second stroke of a multistroke cloud-to-ground flash.

Figure 3 is a plot of density vs wavelength for the daylight exposure taken milliseconds before flash 40.103. Three separate tracings were made milliseconds apart and hand averaged on a light table. The dots in Fig. 3 represent these averaged daylight background data. The solid line is the data corrected by the step-wedge calibration of the densitometer.

The solid line in Fig. 4 is the densitometer tracing (corrected by step-wedge calibration) of the stroke which occurred at the time of the trigger for flash 40.103.

The densitometer tracings are reduced using the calibrations described in Section B. The results for the daylight background and the lightning spectrum are shown in Figs. 5 and 6, respectively. The wavelength scale has also been corrected at this point.

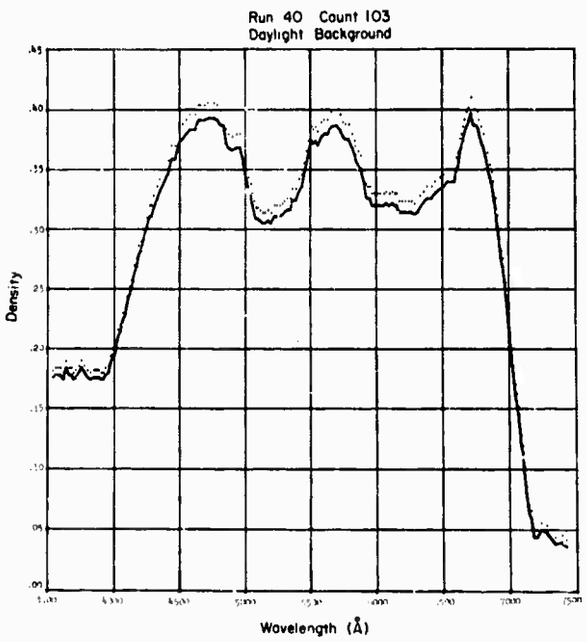

Fig. 3. Density vs wavelength produced by daylight background milliseconds before count 103, run 40. Zero density equals film fog level.

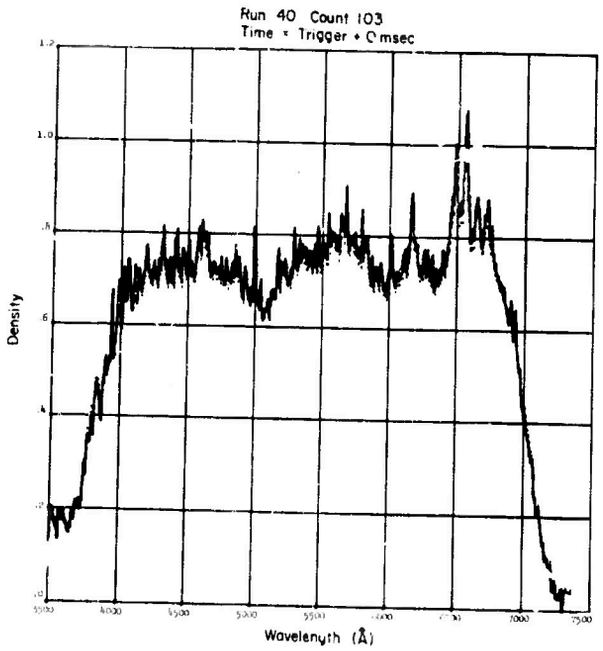

Fig. 4. Density vs wavelength produced by lightning strokes plus daylight background. Zero density equals film fog level.

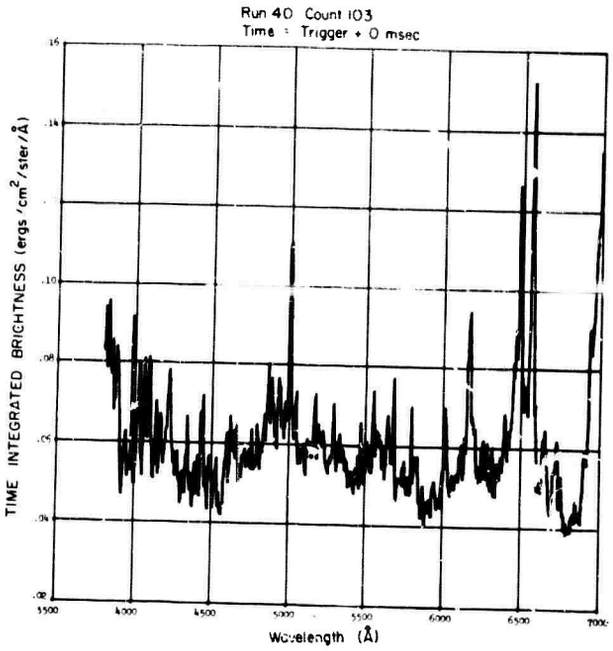

Fig. 6. Lightning spectrum plus inferred daylight spectrum with wavelength scale corrected.

Figure 7 shows the result of subtracting the daylight background from the lightning spectrum.

Figure 8 is the humid-air transmission under Los Alamos weather conditions. (For discussion of atmospheric transmission see the Appendix.) Finally, the spectrum is corrected for humid-air transmission (see Fig. 11), and the dominant radiating species are identified using Charlotte Moore's multiplet designations[6] which are given in Table I.

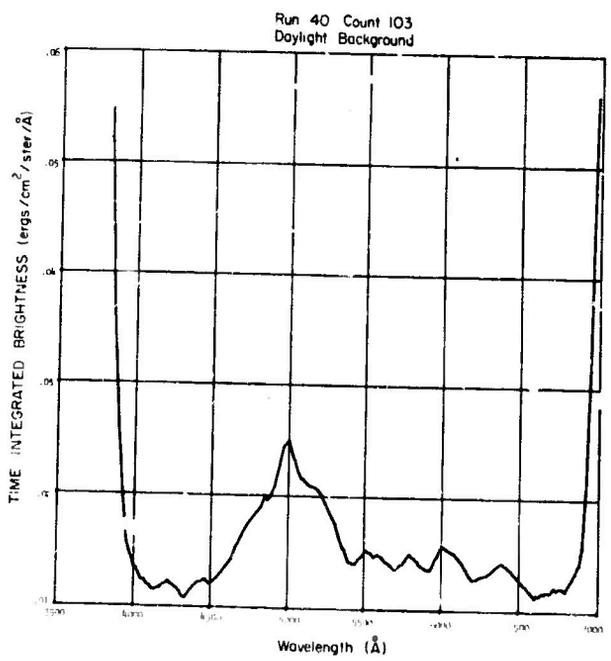

Fig. 5. Inferred daylight background spectrum with wavelength scale corrected.

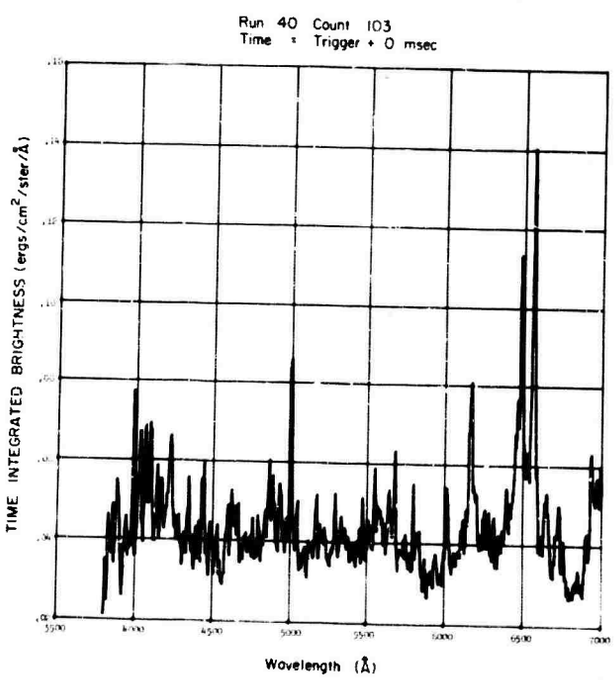

Fig. 7. Spectrum of lightning expressed as brightness vs wavelength of channel image at spectrograph entrance slit.

Table I. Multiplet Designations

Laboratory Wavelength (Å)	Intensity	Term Energy (eV) Low	High	J	Multiplet No.
H		Ionization Potential 13.54 eV			
6562.817	Hα	10.15	12.04	—	2^2P^o-3^2D etc
4861.332	Hβ	10.15	12.69	—	(1) 4^2D etc
4340.468	Hγ	10.15	13.00	—	5^2D etc
4101.737	Hδ	10.15	13.16	—	6^2D etc
3970.074	Hε	10.15	13.26	—	7^2D etc
N I		Ionization Potential 14.49 eV			
4223.04	5	10.29	13.21	2-1/2 - 2-1/2	$3s^4P$-$4p^4P^o$
4230.35	4	10.29	13.21	2-1/2 - 1-1/2	(5)
4224.74	4	10.29	13.21	1-1/2 - 1/2	
4214.73	5	10.29	13.21	1-1/2 - 2-1/2	
4215.92	2	10.26	13.21	1/2 - 1-1/2	
4151.46	12	10.29	13.26	2-1/2 - 1-1/2	$3s^4P$-$4p^4S^o$
4143.42		10.29	13.26	1-1/2 - 1-1/2	(6)
4137.63	7	10.28	13.26	1/2 - 1-1/2	
4109.98	12	10.64	13.65	1-1/2 - 2-1/2	$3s^2P$-$3p^1\ ^2D^o$
4099.94	9	10.63	13.64	1/2 - 1-1/2	(10)
4114.00	6	10.64	13.64	1-1/2 - 1-1/2	
6008.48	10	11.55	13.61	1/2 - 1-1/2	$3p^2S^o$-$4d^2P$
5999.47	6	11.55	13.61	1/2 - 1/2	(16)
6644.96	9	11.71	13.57	3-1/2 - 2-1/2	$3p^4D^o$-$5s^4P$
6653.41	5	11.71	13.56	2-1/2 - 1-1/2	(20)
6656.61	1	11.70	13.56	1-1/2 - 1/2	
6622.53	3	11.71	13.57	2-1/2 - 2-1/2	
6637.01	4	11.70	13.56	1-1/2 - 1-1/2	
6646.52	2	11.70	13.56	1/2 - 1/2	
6482.74	9	11.71	13.62	3-1/2 - 4-1/2	$3p^4D^o$-$4d^4P$
6484.88	9	11.71	13.61	2-1/2 - 3-1/2	(21)
6483.75	3	11.70	13.61	1-1/2 - 2-1/2	
6431.73	2	11.70	13.60	1/2 - 1-1/2	
6505.45	0	11.71	13.61	3-1/2 - 3-1/2	
6499.52	3	11.71	13.61	2-1/2 - 2-1/2	
6491.28	3	11.70	13.60	1-1/2 - 1-1/2	
6723.12	9	11.79	13.63	2-1/2 - 2-1/2	$3p^4P^o$-$4d^4P$
6733.48	6	11.79	13.62	1/2 - 1/2	(31)
6706.20	4	11.79	13.63	1-1/2 - 2-1/2	
6741.29	3	11.79	13.62	1-1/2 - 1/2	
O I		Ionization Potential 13.56 eV			
6158.19	18	10.69	12.70	3 -	3^5P-4^5D^o
6156.78	17	10.69	12.70	2 -	(10)
6155.99	16	10.69	12.70	1 -	
N II		Ionization Potential 29.49 eV			
5679.56	10	18.40	20.58	2 - 3	$3s^3P^o$-$3p^3D$
5666.64	8	18.39	20.58	1 - 2	(3)
5676.02	6	18.38	20.56	0 - 1	
5710.76	6	18.40	20.56	2 - 2	
5686.21	6	18.39	20.56	1 - 1	
5730.67	4	18.40	20.56	2 - 1	
5045.098	8	18.40	20.85	2 - 1	$3s^3P^o$-$3p^3S$
5010.620	6	18.39	20.85	1 - 1	(4)
5002.692	2	18.38	20.85	0 - 1	
4630.537	10	18.40	21.07	2 - 2	$3s^3P^o$-$3p^3P$
4613.868	6	18.39	21.06	1 - 1	(5)
4643.086	8	18.40	21.06	2 - 1	
4621.392	7	18.39	21.06	1 - 0	
4601.478	8	18.39	21.07	1 - 2	
4607.153	7	18.39	21.06	0 - 1	

Laboratory Wavelength (Å)	Intensity	Term Energy (eV) Low	High	J	Multiplet No.
N II (cont.)		Ionization Potential 29.49 eV			
3994.996	10	18.42	21.51	1 - 2	$3s^1P^o$-$3p^1D$ (12)
4447.033	10	20.32	23.10	1 - 2	$3p^1P$-$3d^1D^o$ (15)
5005.140	10	20.58	23.04	3 - 4	$3p^3D$-$3d^3P^o$
5001.469	8	20.56	23.03	2 - 3	(19)
5001.128	7	20.56	23.02	1 - 2	
5025.665	6	20.58	23.03	3 - 3	
5016.387	5	20.56	23.02	2 - 2	
5040.76	0	20.58	23.02	3 - 1	
4607.315	7	20.85	23.31	1 - 2	$3p^3S$-$3d^3P^o$
4994.358	6	20.85	23.32	1 - 1	(24)
4987.377	4	20.85	23.32	1 - 0	
5941.67	8	21.07	23.15	2 - 3	$3p^3P$-$3d^3D^o$
5931.79	7	21.06	23.14	1 - 2	(28)
5927.82	4	21.06	23.14	0 - 1	
5952.39	3	21.07	23.14	2 - 2	
5940.25	2	21.06	23.14	1 - 1	
5960.93	0	21.07	23.14	2 - 1	
4227.749	3n	21.51	24.43	2 - 1	$3p^1D$-$4s^1P^o$ (33)
6167.82	4	23.04	25.04	4 - 3	$3d^3P^o$-$4p^3D$
6173.40	3	23.03	25.03	3 - 2	(36)
6170.16	1	23.02	25.03	2 - 1	
6136.9	0	23.03	25.04	3 - 3	
6150.9	0	23.02	25.03	2 - 2	
6114.6	0	23.02	25.03	2 - 3	
4041.321	5n	23.04	26.10	4 - 5	$3d^3F^o$-$4f^3G$
4043.537	3n	23.03	26.08	3 - 4	(39)
4035.087	4n	23.02	26.08	2 - 3	
4057.00	1	23.04	26.08	4 - 4	
4044.75	1	23.03	26.08	3 - 3	
4432.739	6n	23.31	26.10	2 - 3	$3d^3P^o$-$4f^3D$
4441.99	3n	23.32	26.10	1 - 2	(55)
4433.48	2n	23.32	26.11	0 - 1	
4431.82	0	23.31	26.10	2 - 2	
4427.97	2	23.32	26.11	1 - 1	
4694.55	3n	23.47	26.10	1 - 2	$3d^1P^o$-$4f^3D$ (61)
4677.93	3n	23.47	26.11	1 - 2	$3d^1P^o$-$4f^1D$ (62)
5012.026	2	(25.38	27.84)	3 - 3	$3s^5P$-$3p^5P^o$
5005.140	10	(25.37	27.84)	2 - 2	(64)
4997.23	0	(25.37	27.84)	1 - 1	
5023.11	2	(25.38	27.84)	3 - 2	
5011.24	1	(25.37	27.84)	2 - 1	
4994.358	6	(25.37	27.84)	2 - 3	
4991.22	2	(25.37	27.84)	1 - 2	
4718.43	2	(27.61	30.23)	4 - 4	$3p^5D^o$-$3d^5D$
4709.45	1	(27.61	30.23)	3 - 3	(68)
4702.57	0	(27.60	30.22)	2 - 2	
4721.59	0	(27.61	30.23)	4 - 3	
4712.13	0	(27.61	30.22)	3 - 2	
4704.33	0	(27.60	30.22)	2 - 1	
4698.62	0	(27.60	30.22)	1 - 0	
4706.41	0	(27.61	30.23)	3 - 4	
4700.12	0	(27.60	30.23)	2 - 3	
4695.91	1	(27.60	30.22)	1 - 2	

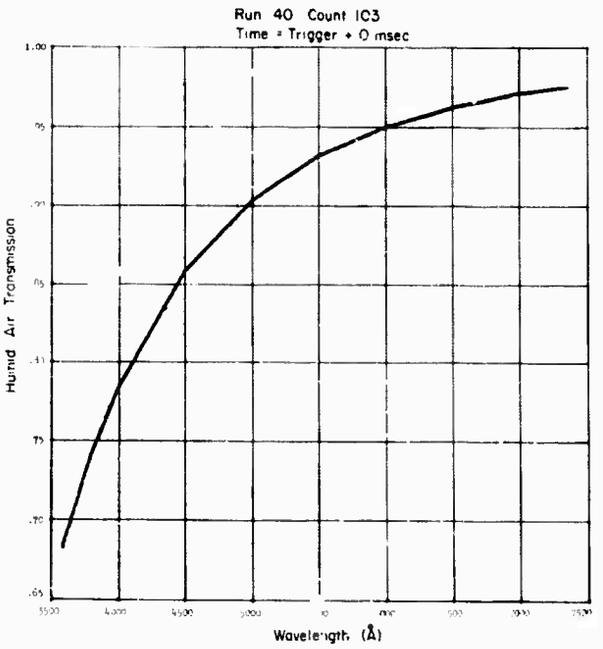

Fig. 8. Humid-air transmission for 7-km observation path under Los Alamos weather conditions.

D. Results

The results are presented here in the form of fully reduced spectra whose strongest and most reproducible (from stroke to stroke) features are identified. These spectra are presented in Figs. 9 through 25 as plots of wavelength vs time-integrated flux at the entrance pupil of the spectrograph. Each is identified by a run and count number. The time given is that at which the spectrum was obtained measured relative to the trigger provided by the collimated photoelectric H_α channels. The records of the Los Alamos weather station were used to calculate the atmospheric selective transmission as described in the Appendix. The range of the stroke was measured by photographic triangulation.[7] The spectral flux is integrated over wavelength from 3900 to 6900 Å, and after rain transmission correction this result is used to calculate the efficiency of conversion of electrical energy to visible radiation in the channel.

It must be pointed out that the time-integrated flux is that originating from a length of channel whose vertical component is ℓ. The vertical length of the channel over which the spectrum is spatially integrated is dependent on range and is given by $\ell = 0.9\ R$ meters, where R is the range in kilometers.

Spectra were obtained for first return strokes, subsequent return strokes, and continuing luminosities.

E. Discussion of Results

In the data reduction the most difficult problem was to prove that the continuum, inferred from the slitless spectra, was indeed true continuum and not scattered light.[8] This problem was solved during the summer of 1966 by operating the same spectrograph as a time-resolving slit instrument. On the whole, the slit and slitless spectra show features similar to those described above. While the results of the slit spectra are still preliminary, I can make the following statements regarding the two types of spectra:

(1) Neither the time-resolved slitless spectra nor the time-resolved slit spectra show a bandhead at 3914 Å.

(2) For the slitless spectra, the image of the lightning channel at the entrance aperture may, indeed, be regarded as the entrance slit; i.e. the spectra presented here are free from errors due to light scattered from points at large angular distances from the channel. This conclusion is drawn from the structural similarity of continua of the slit and slitless spectra in those intervals (3800 to 4000 Å, 4800 to 5200 Å, and 6800 to 7000 Å) in which the spectrograph-film sensitivity is changing quickly as a function of wavelength.

(3) Linewidths for the slit spectra are narrower than those for the slitless spectra. This may be due to light scattered, reflected, or emitted close to the channel or to light scattered at small angles near the propagation path to the detector. However, such scattering is not sufficient at large distances from the channel to contradict conclusion (2), and limits the interpretation of the slitless spectra only insofar as it prevents the inference of linewidths from them.

The slitless spectra may be classified as: (1) first return strokes, (2) subsequent return strokes, and (3) continuing luminosities, each with different spectral characteristics. The descriptions of each follow.

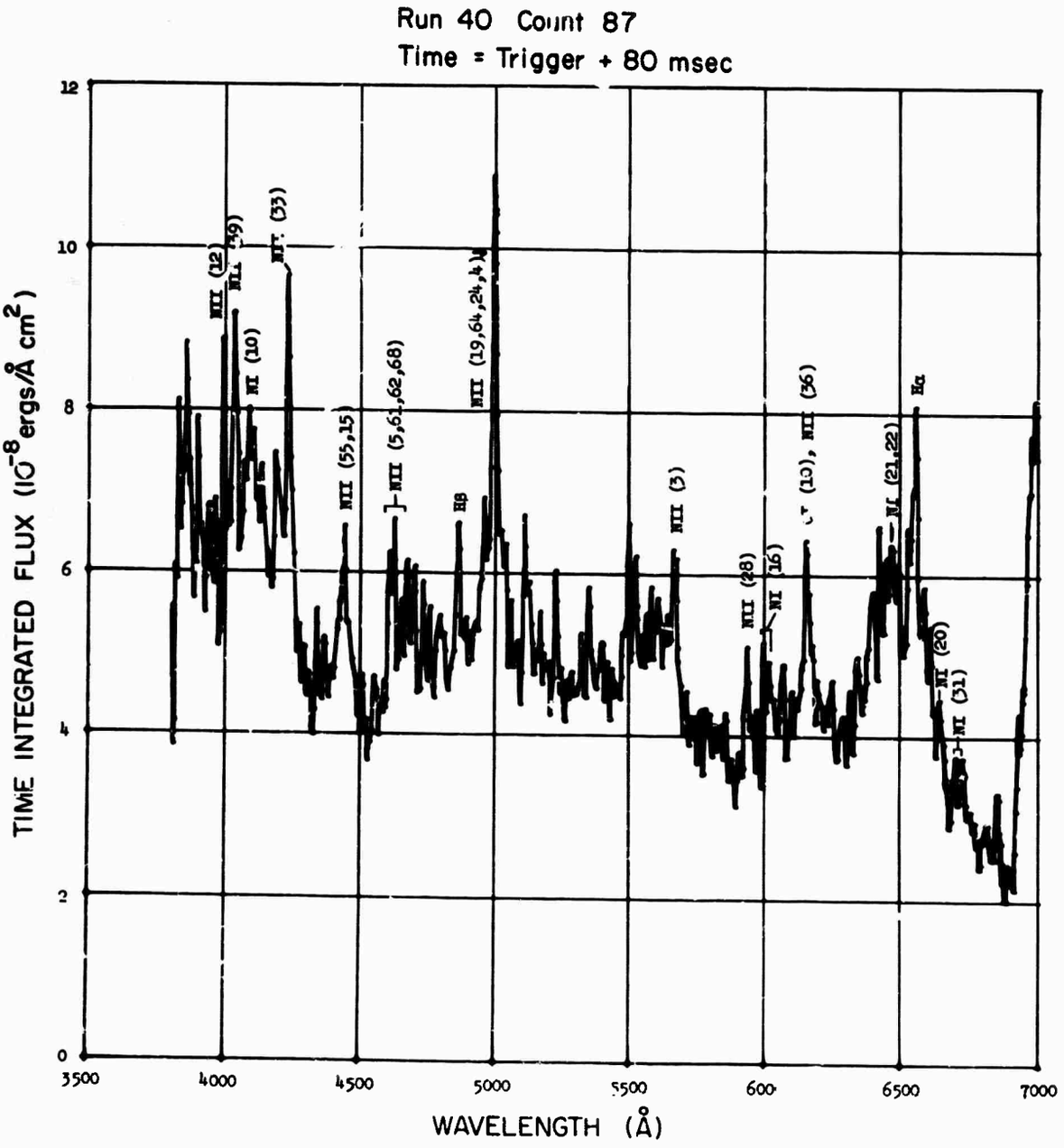

Fig. 9. Spectrum (taken at twilight) of first return stroke. Electrical energy deposited = 3.3×10^5 joule/meter. Rainfall transmission = 8.7×10^{-3}. Visible energy radiated = 2.0×10^3 joule/meter, corrected for rainfall transmission. Range = 10 km.

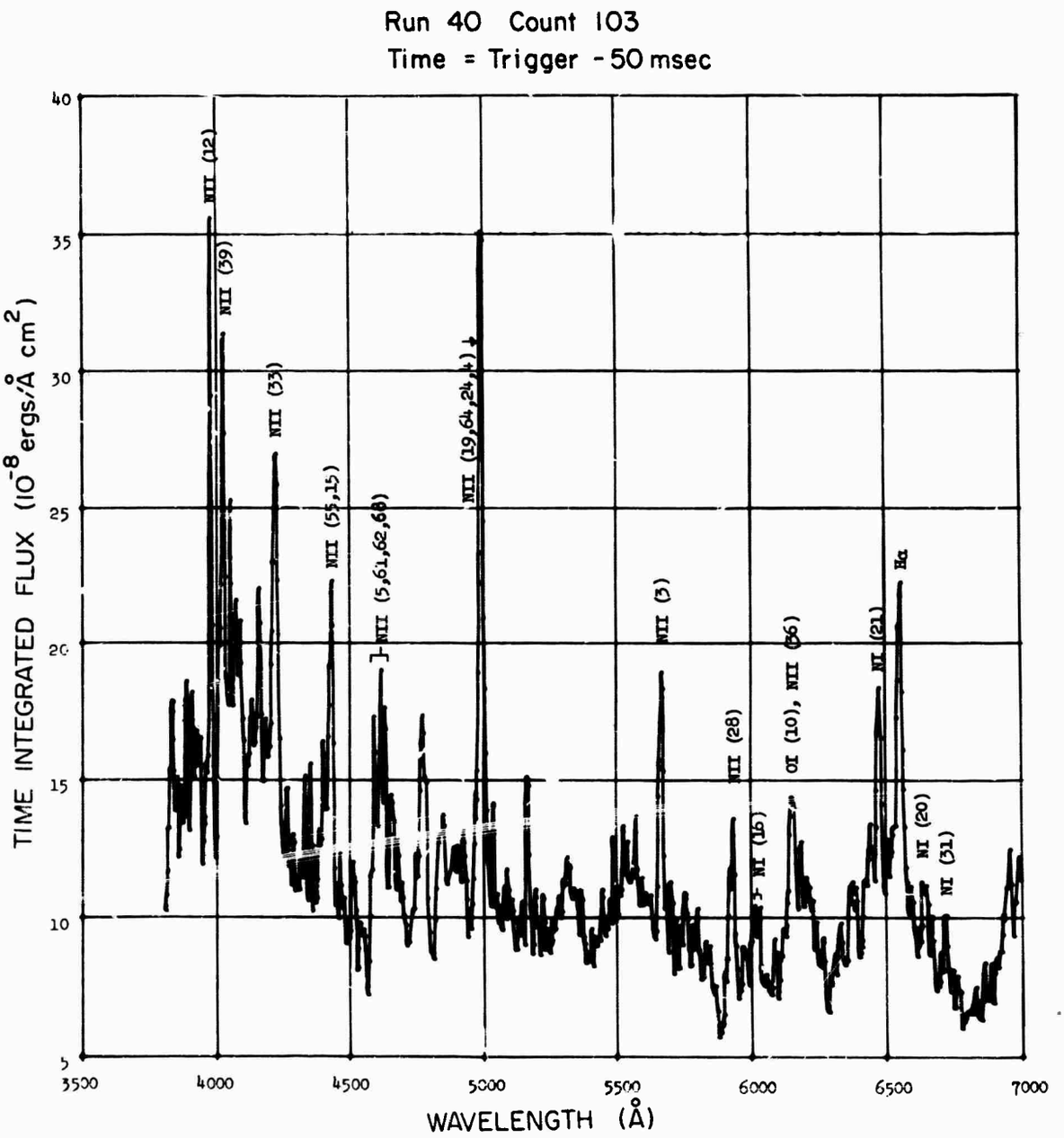

Fig. 10. Spectrum (taken at twi[illegible]ht) of first return stroke. Electrical energy deposited is unknown. Rain transmission = 3.6×10^{-2}. Visible energy radiated = 7.7×10^{2} joule/meter, corrected for rainfall transmission. Range = 7 km.

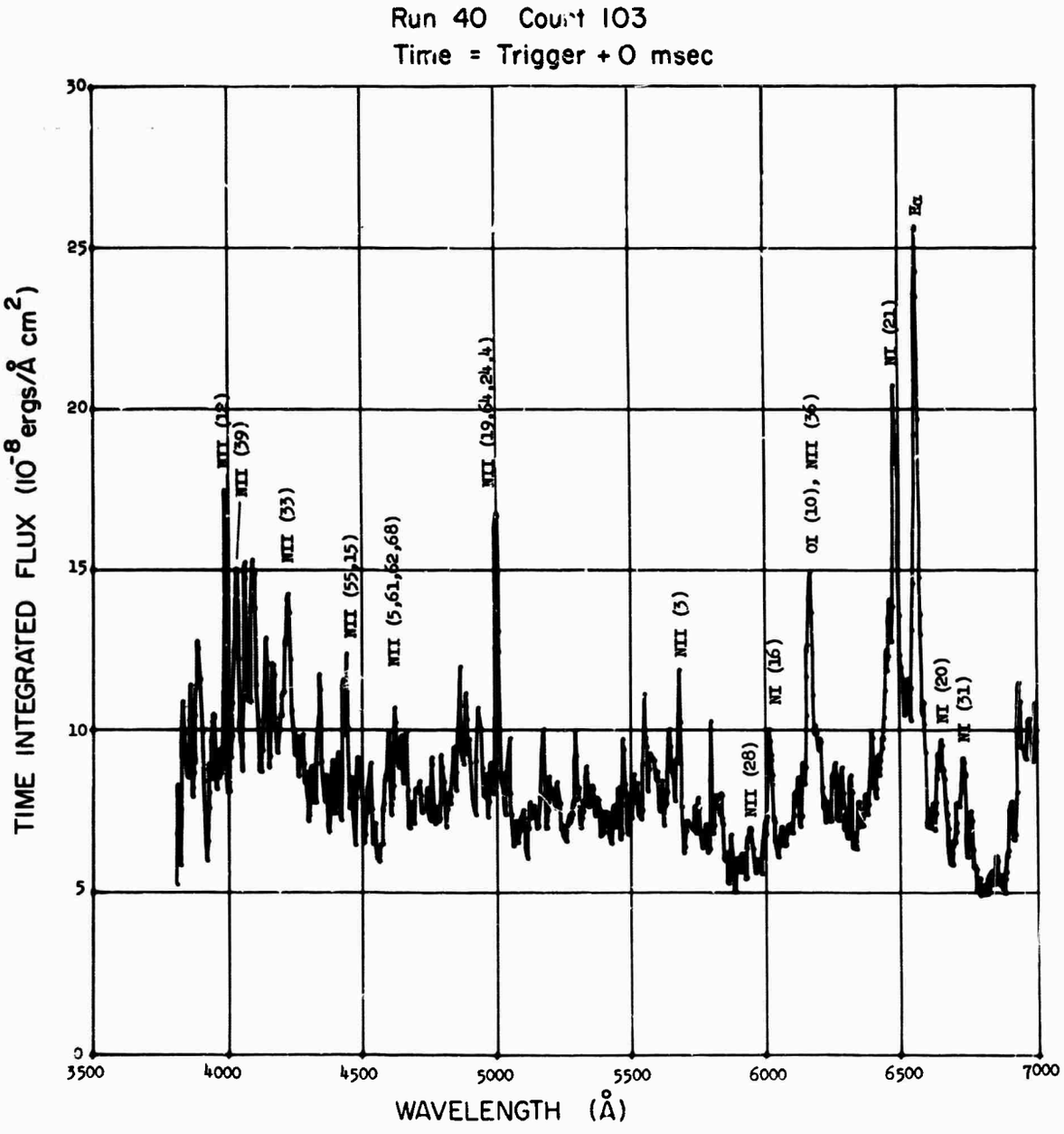

Fig. 11. Spectrum (taken at twilight) of subsequent return stroke. Electrical energy deposited is unknown. Rain transmission = 3.6×10^{-2}. Visible energy radiated = 5.6×10^{2} joule/meter, corrected for rainfall transmission. Range = 7 km.

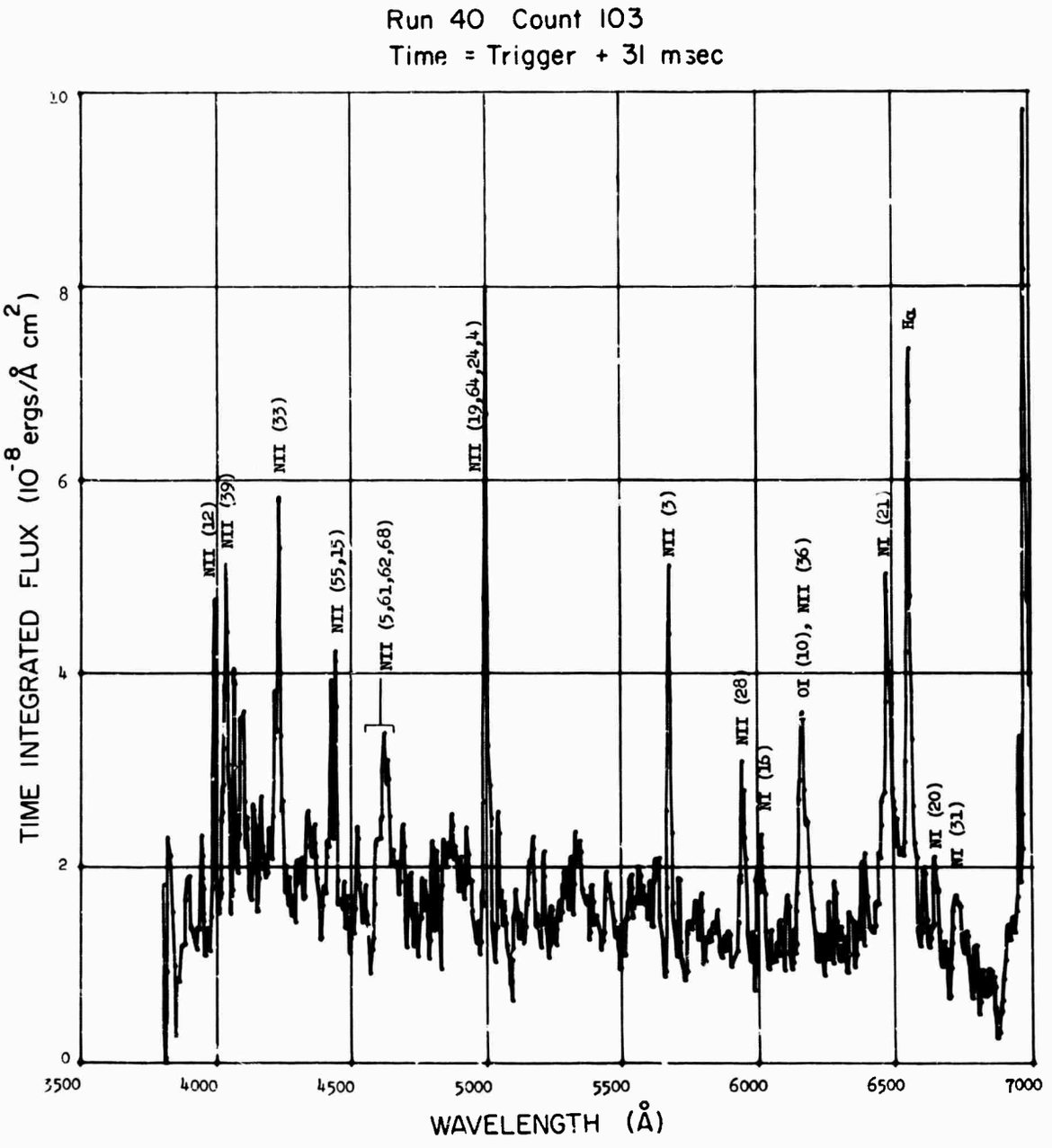

Fig. 12. Spectrum (taken at twilight) of subsequent return stroke. Electrical energy deposited is unknown. Rain transmission = 3.6×10^{-2}. Visible energy radiated = 4.2×10^{1} joule/meter, corrected for rainfall transmission. Range = 7 km.

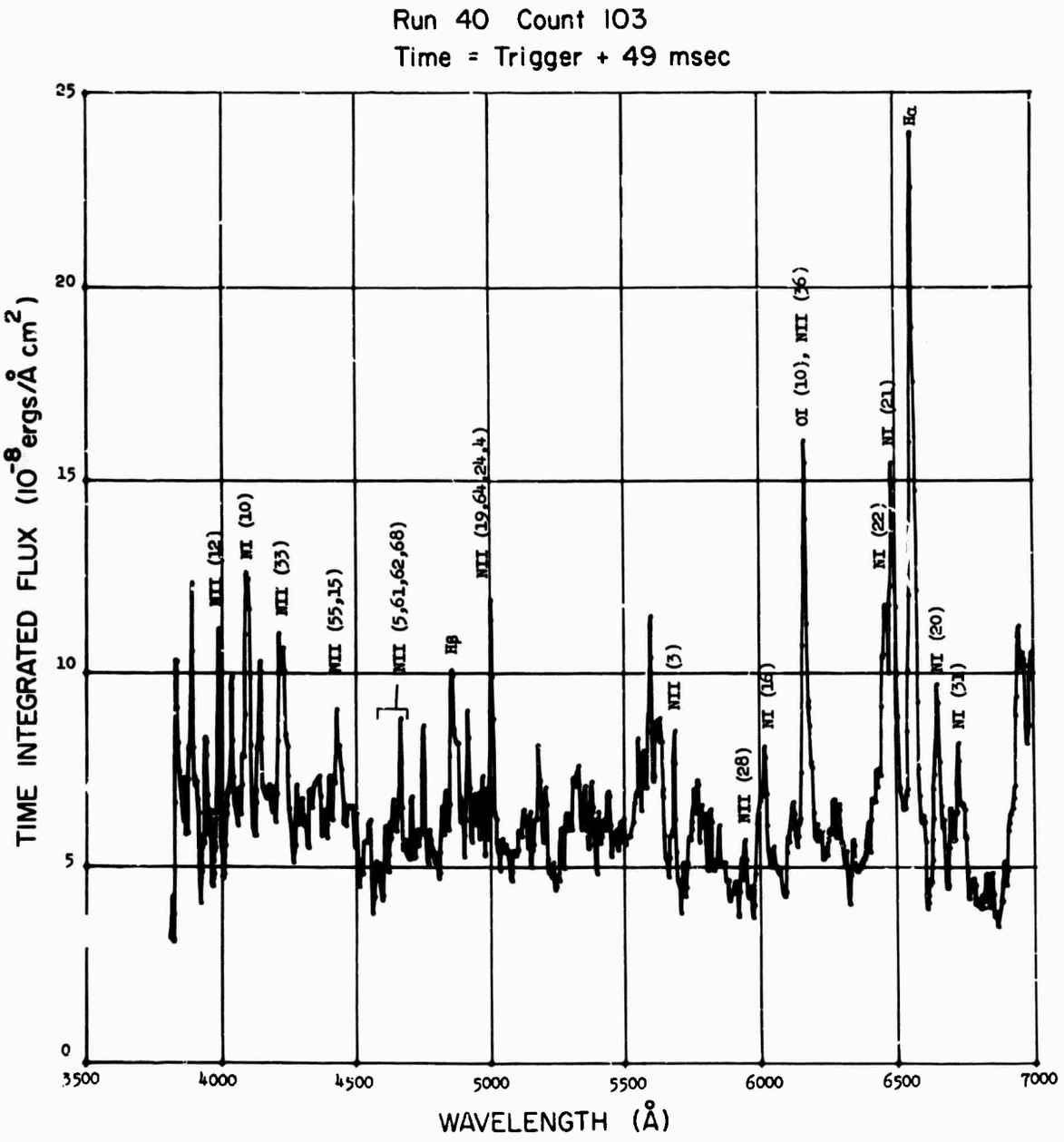

Fig. 13. Spectrum (taken at twilight) of subsequent return stroke. Electrical energy deposited = 4.0×10^4 joule/meter. Rain transmission = 3.6×10^{-2}. Visible energy radiated = 4.2×10^2 joule/meter, corrected for rainfall transmission. Range = 7 km.

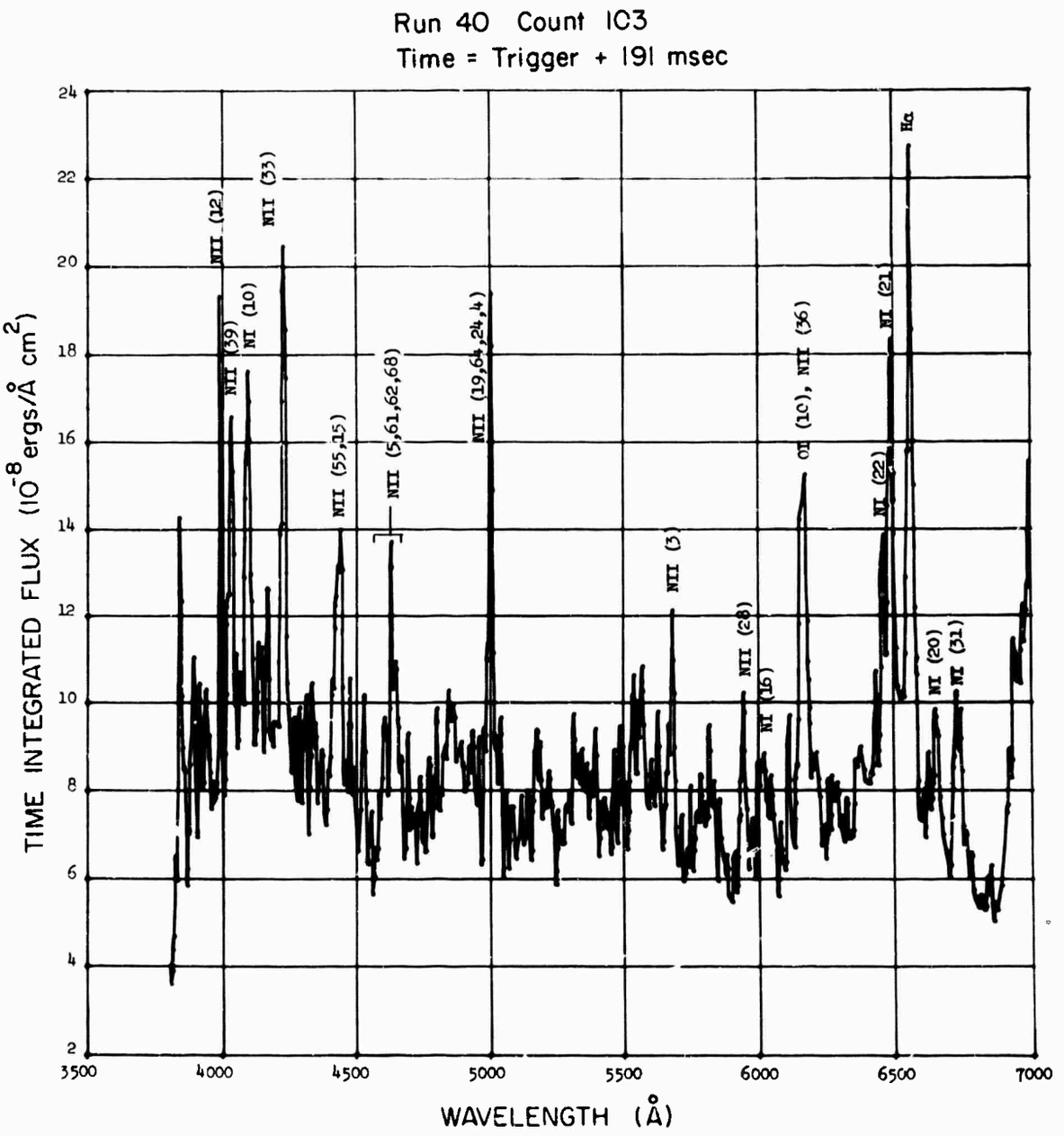

Fig. 14. Spectrum (taken at twilight) of subsequent return stroke. Electrical energy deposited = 9.0×10^4 joule/meter. Rain transmission = 3.6×10^{-2}. Visible energy radiated = 5.7×10^2 joule/meter, corrected for rainfall transmission. Range = 7 km.

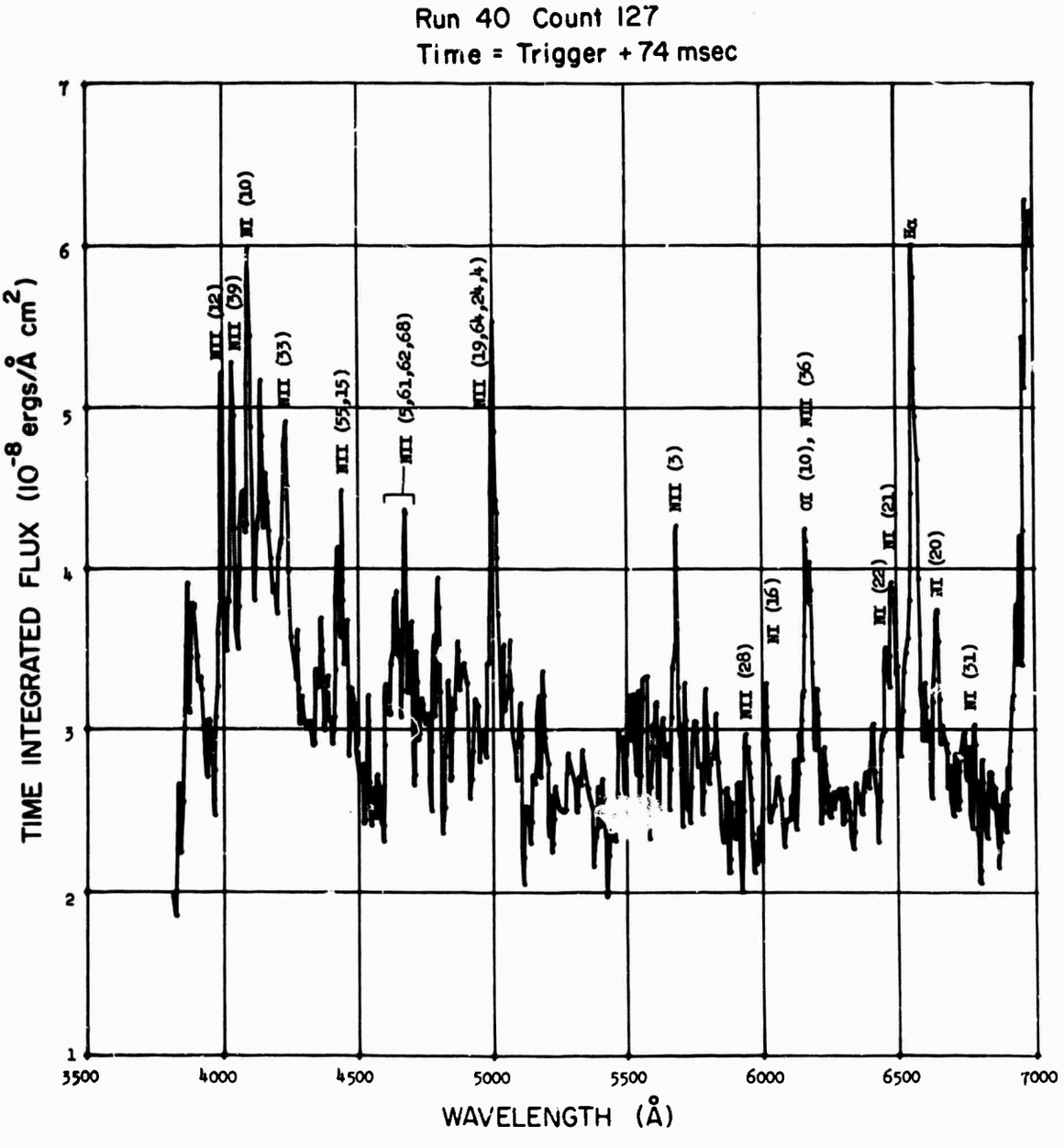

Fig. 15. Spectrum (taken at twilight) of first return stroke. Electrical energy deposited = 3.2×10^4 joule/meter. Rain transmission = 3.3×10^{-2}. Visible energy radiated = 2.3×10^2 joule/meter, corrected for rainfall transmission. Range = 7.2 km.

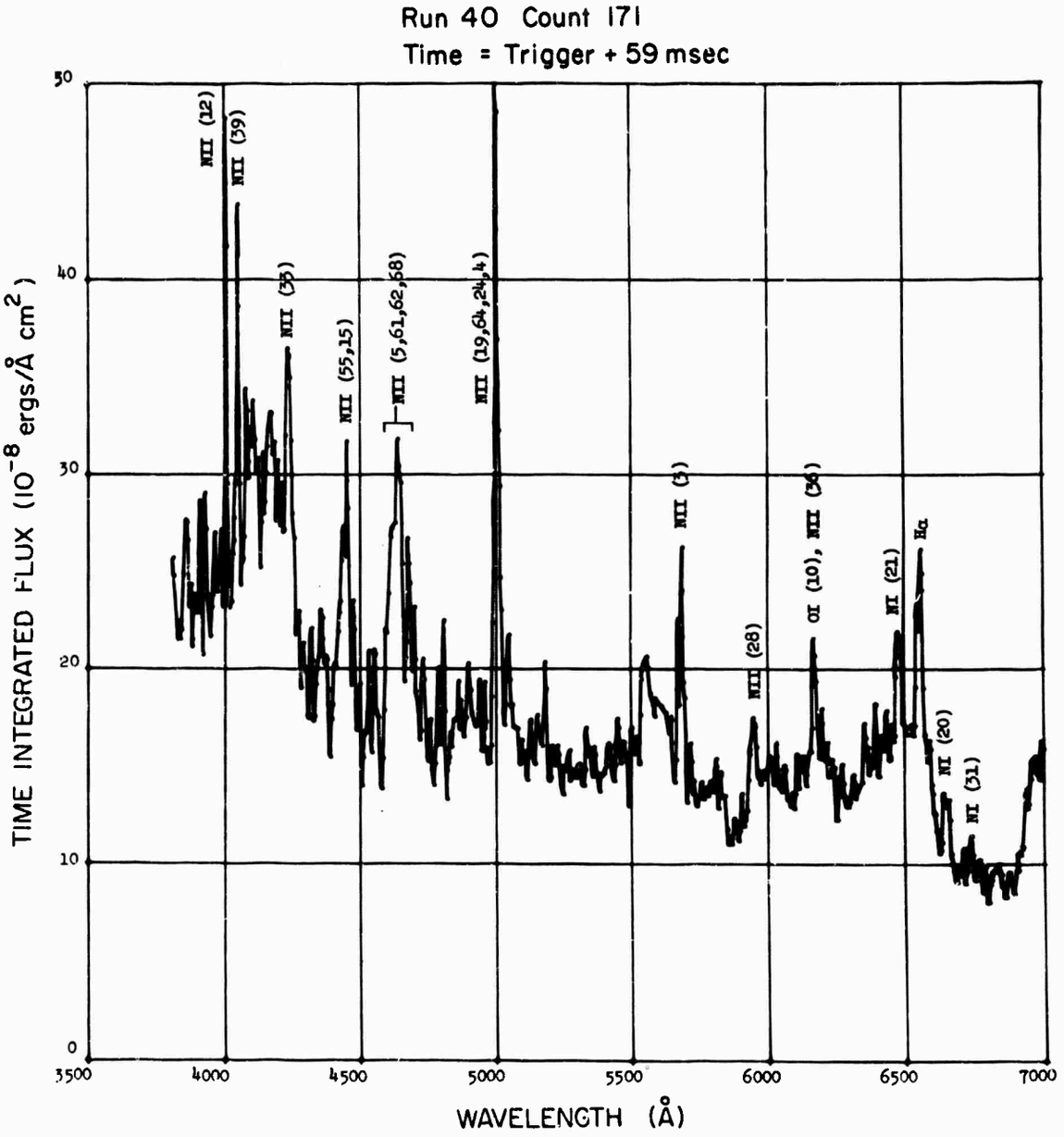

Fig. 16. Spectrum (taken at twilight) of first return stroke. Electrical energy deposited = 2.1 x 10^4 joule/meter. Rain transmission = 1.1 x 10^{-1}. Visible energy radiated = 2.3 x 10^2 joule/meter, corrected for rain transmission. Range = 4.0 km.

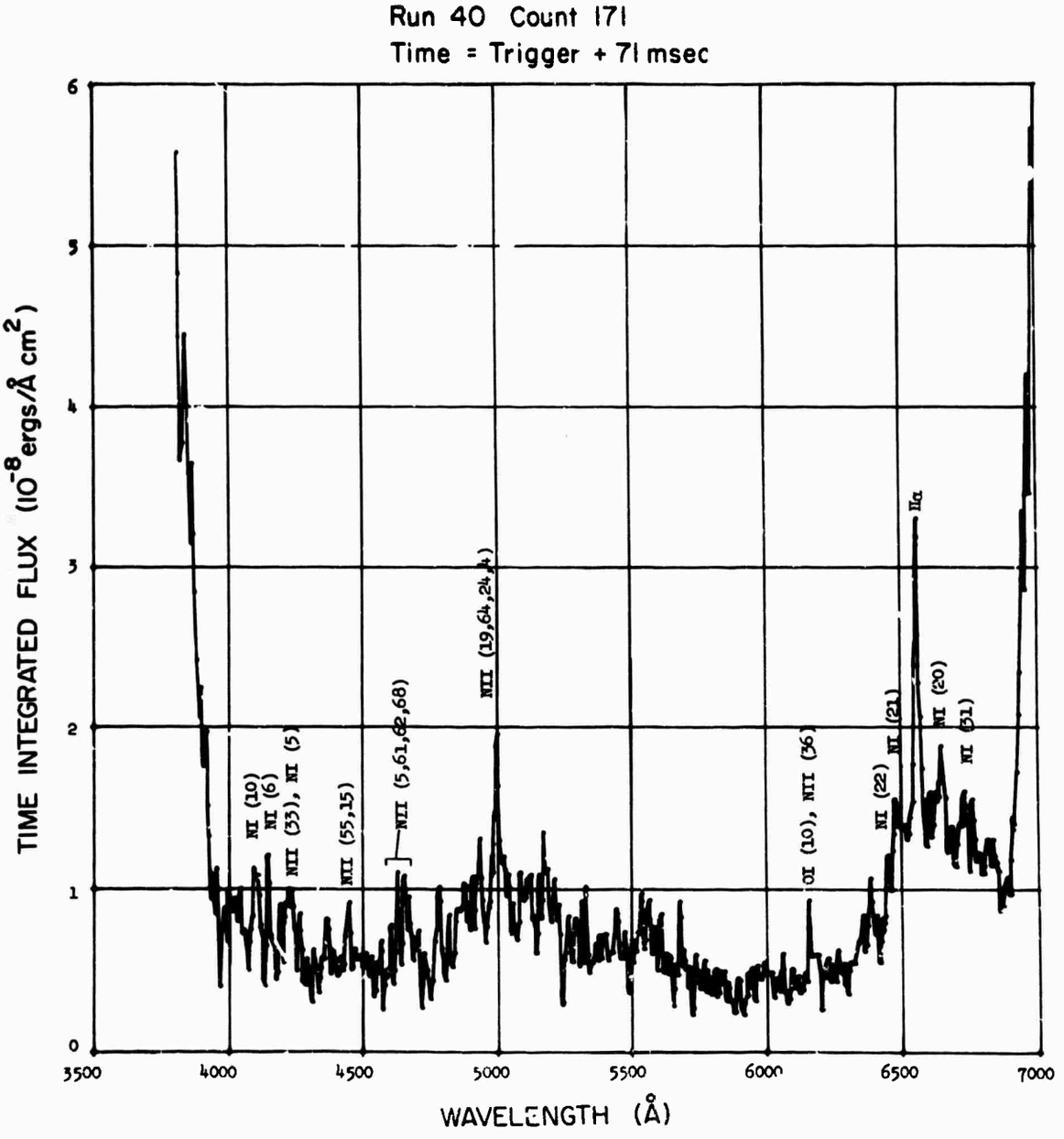

Fig. 17. Spectrum (taken at twilight) of subsequent return stroke which results in a continuing luminosity. Electrical energy deposited is unknown. Rain transmission = 1.1×10^{-1}. Visible energy radiated = 9.8 joule/meter, corrected for rain transmission. Range = 4.0 km.

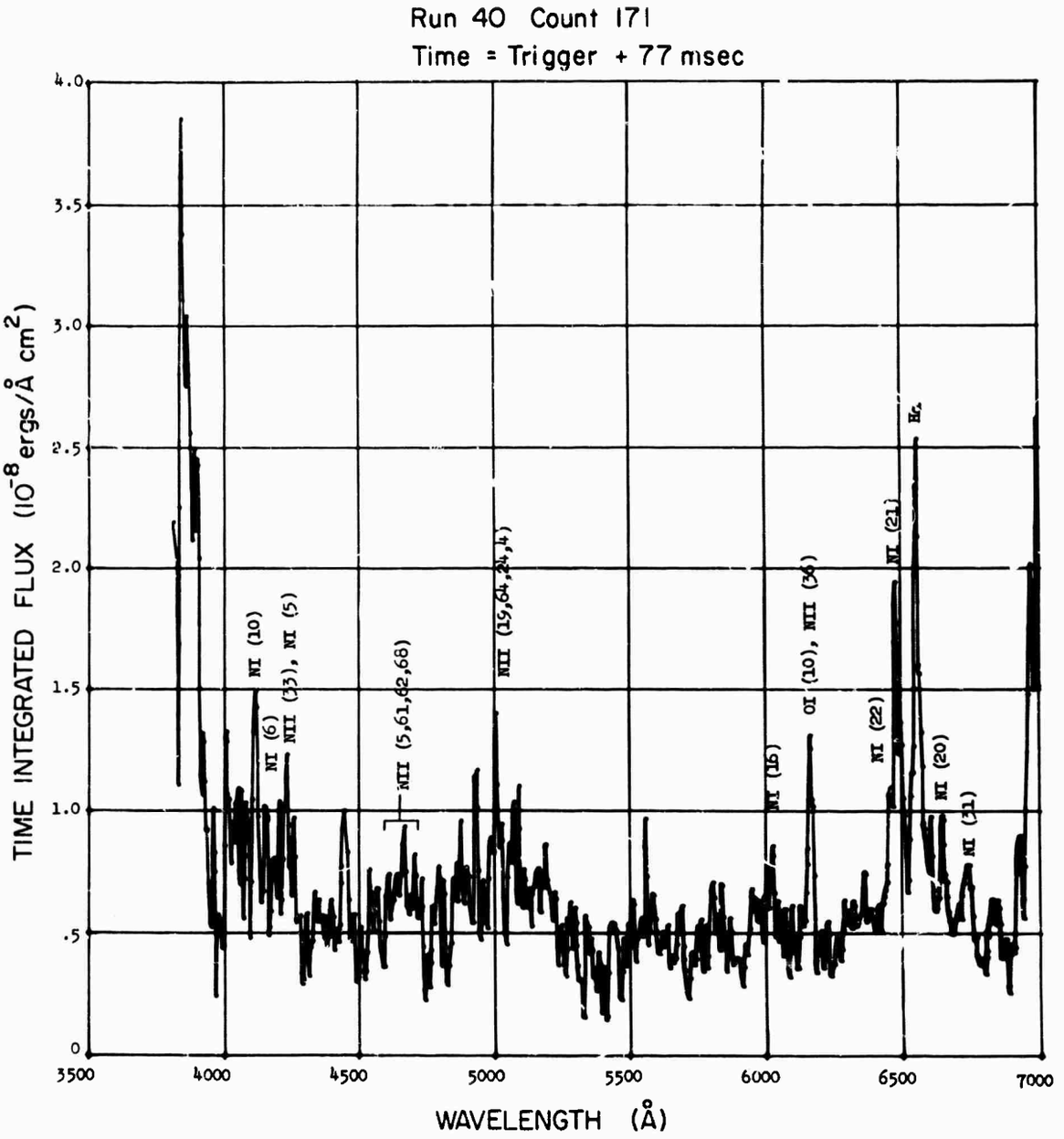

Fig. 18. Spectrum (taken at twilight) of continuing luminosity. Electrical energy deposited is unknown. Rain transmission = 1.1×10^{-1}. Visible energy radiated = 7.9 joule/meter, corrected for rain transmission. Range = 4.0 km.

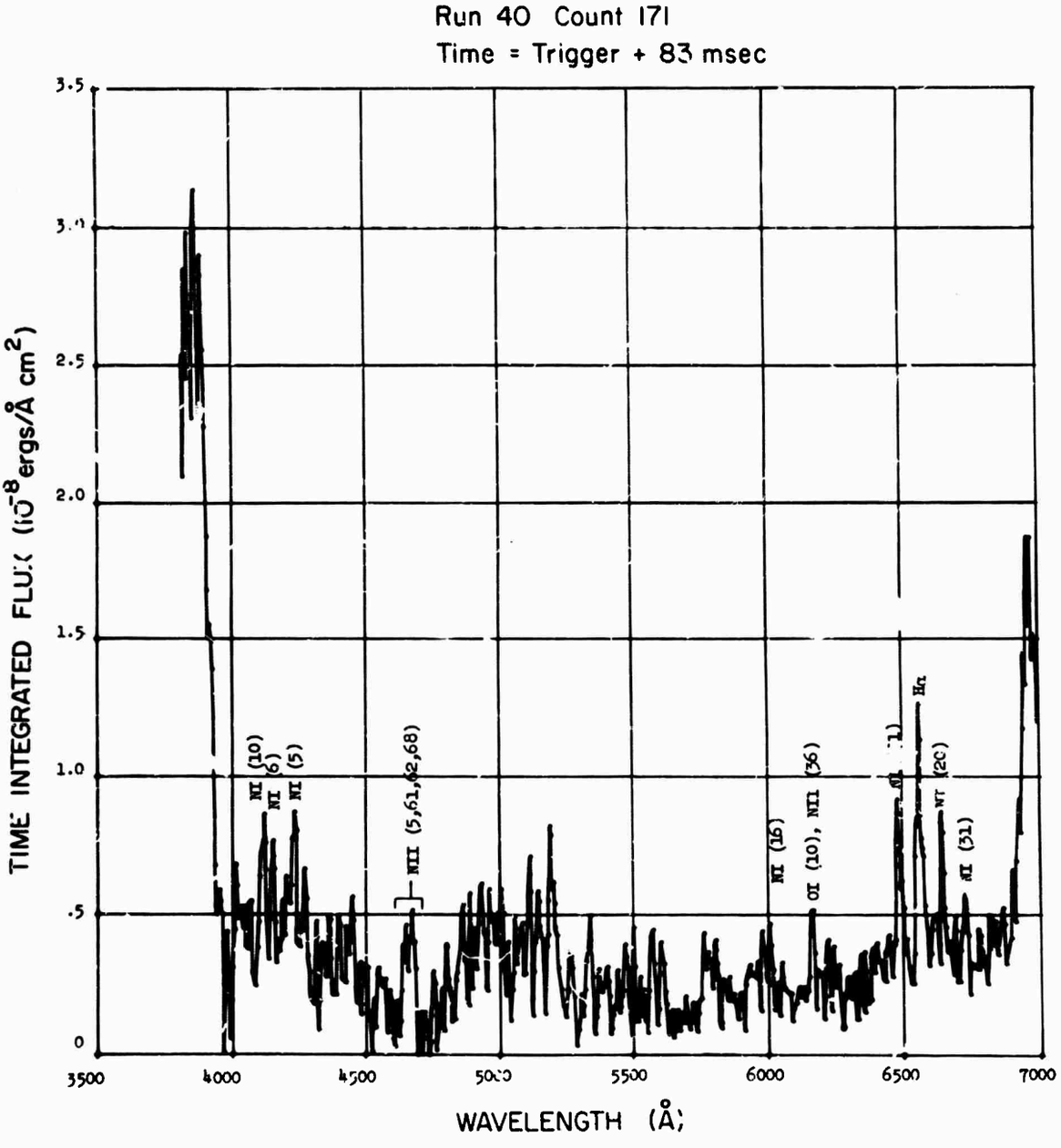

Fig. 19. Spectrum (taken at twilight) of a continuing luminosity. Electrical energy deposited is unknown. Rain transmission = 1.1×10^{-1}. Visible energy radiated = 4.3 joule/meter, corrected for rain transmission. Range = 4.0 km.

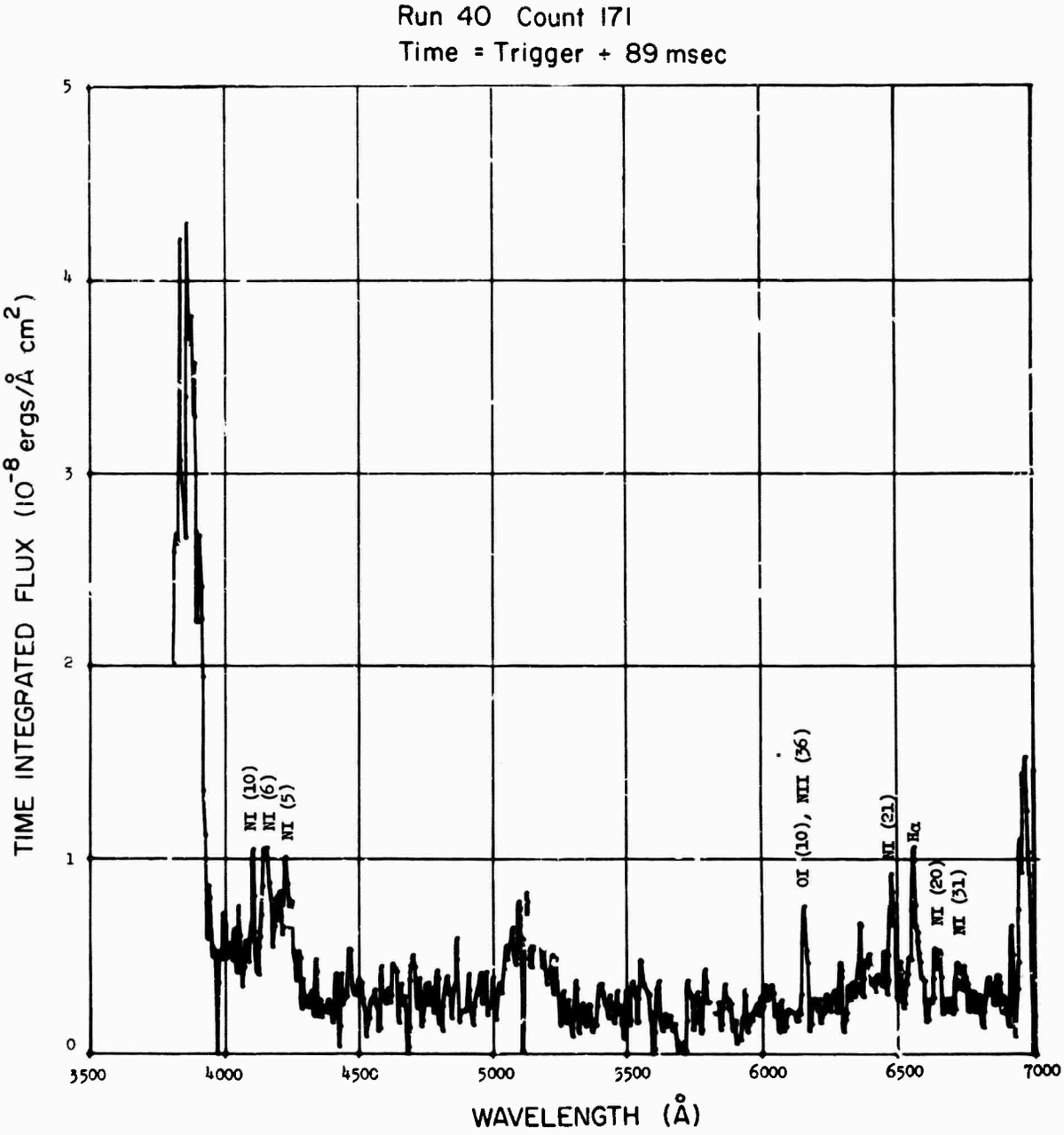

Fig. 20. Spectrum (taken at twilight) of a continuing luminosity. Electrical energy deposition is unknown. Rain transmission = 1.1 x 10^{-2}. Visible energy radiated = 4.5 joule/meter, corrected for rain transmission. Range = 4.0 km.

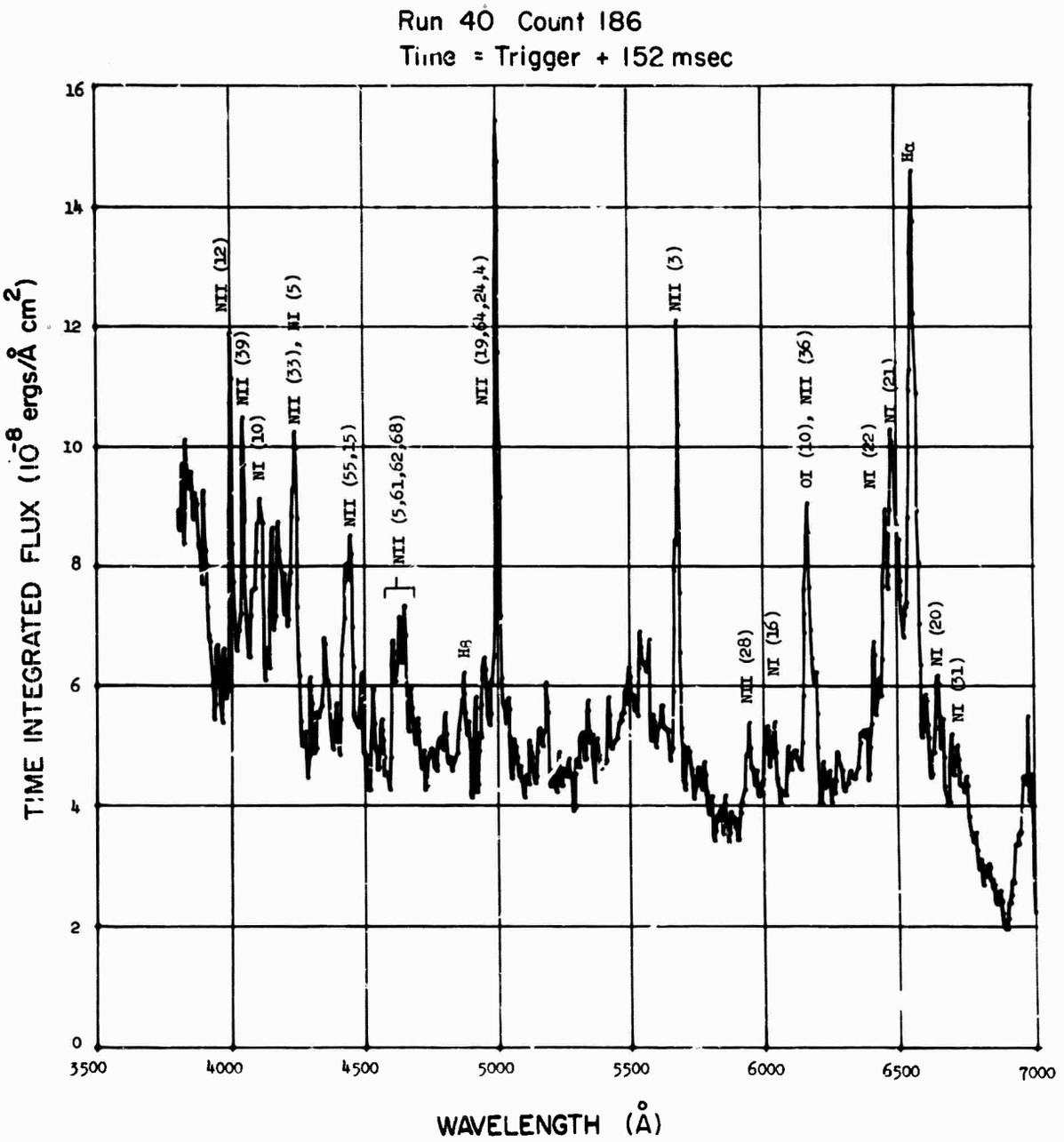

Fig. 21. Spectrum (taken at twilight) of first return stroke. Electrical energy deposited = 2.2×10^4 joule/meter. Rain transmission = 1.5×10^{-1}. Visible energy radiated = 5.9×10^1 joule/meter, corrected for rain transmission. Range = 4.6 km.

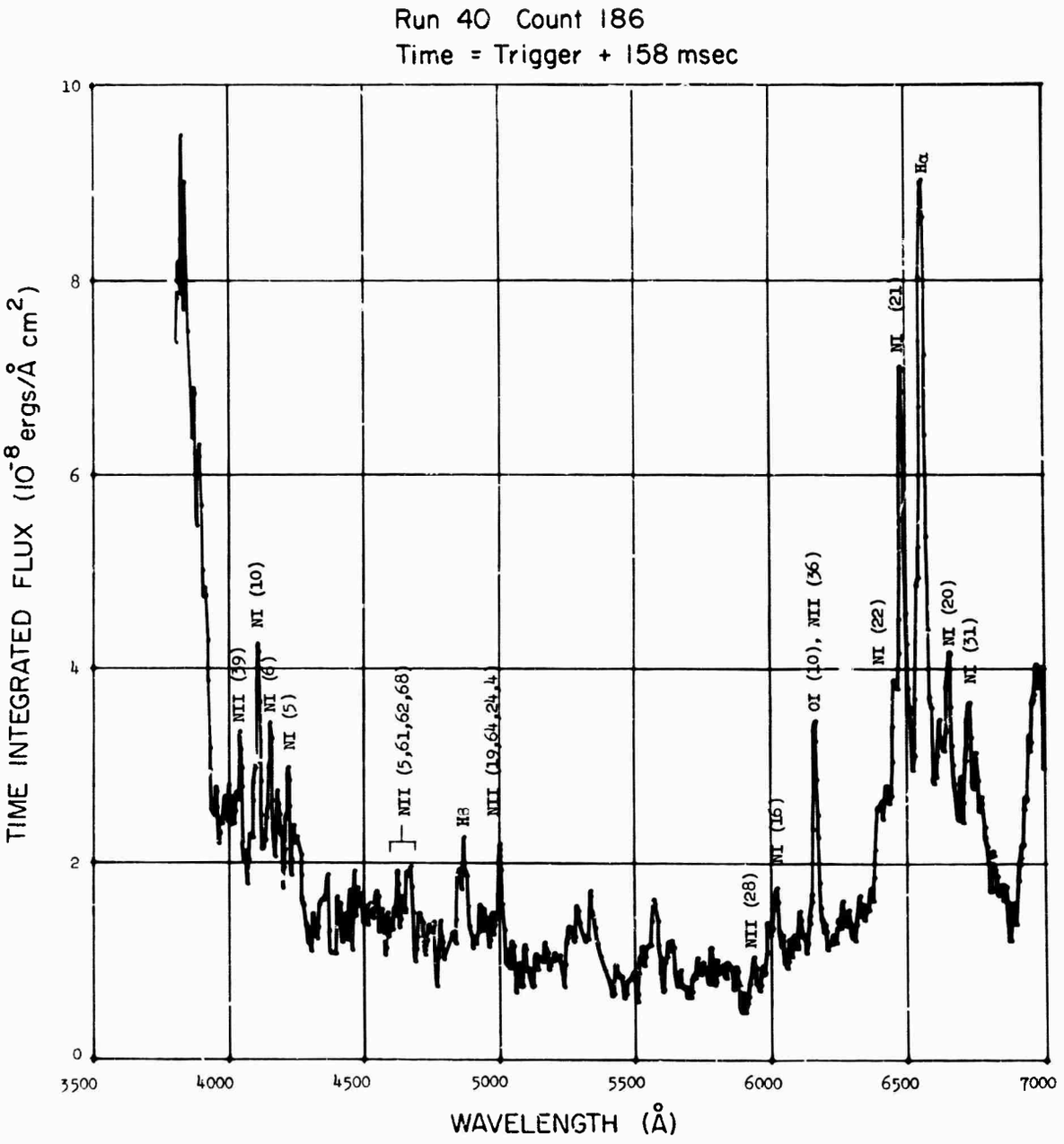

Fig. 22. Spectrum (taken at night) of continuing luminosity. Electrical energy deposition is unknown. Rain transmission = 1.5×10^{-1}. Visible energy radiated = 1.9×10^{1} joule/meter, corrected for rain transmission. Range = 4.6 km.

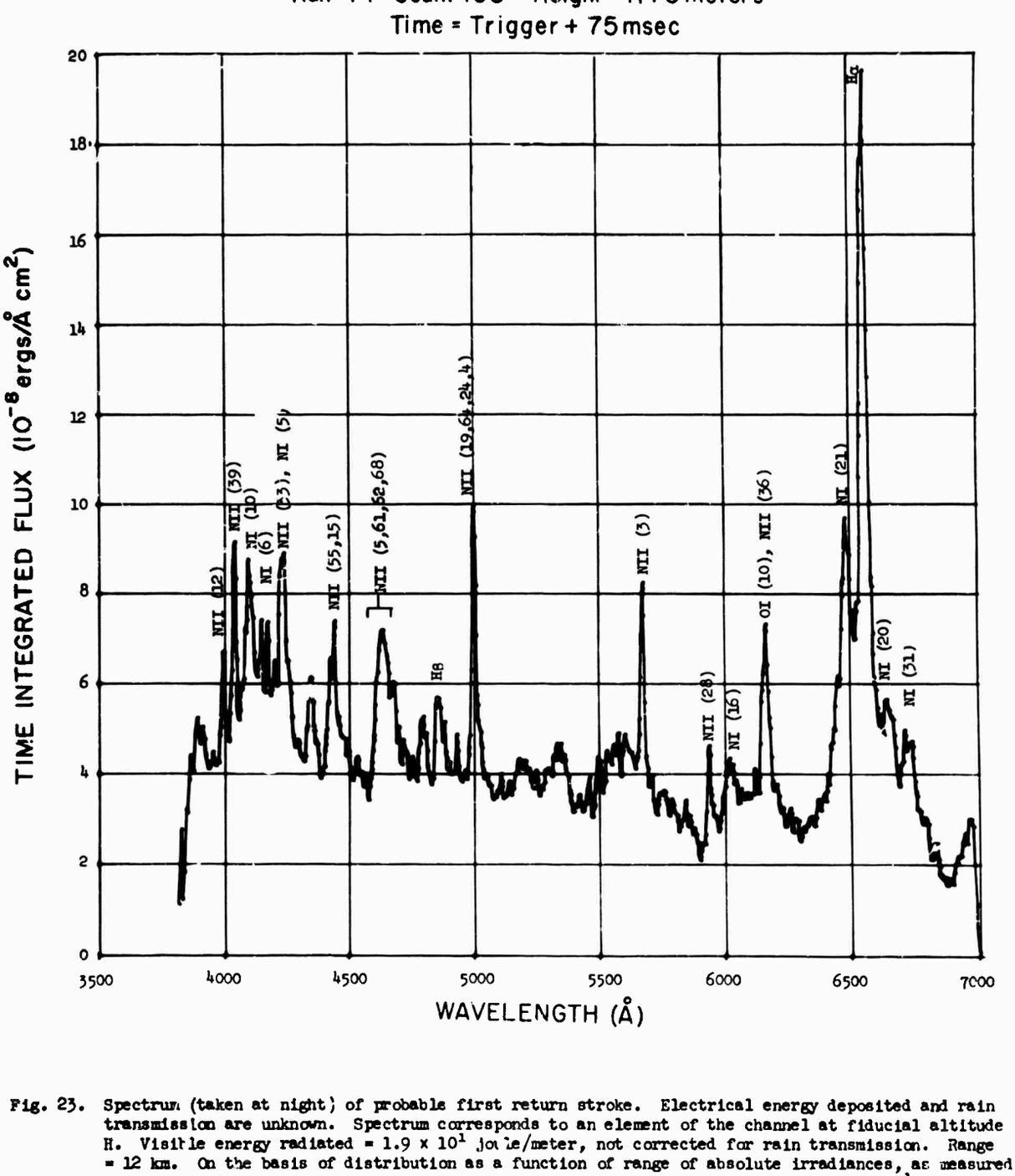

Fig. 23. Spectrum (taken at night) of probable first return stroke. Electrical energy deposited and rain transmission are unknown. Spectrum corresponds to an element of the channel at fiducial altitude H. Visible energy radiated = 1.9×10^{1} joule/meter, not corrected for rain transmission. Range = 12 km. On the basis of distribution as a function of range of absolute irradiances, as measured by collimated photometers, the rain extinction coefficient is estimated to be 0.15 km^{-1}. Thus, estimated rain transmission for this count is $\sim 1.7 \times 10^{-2}$.

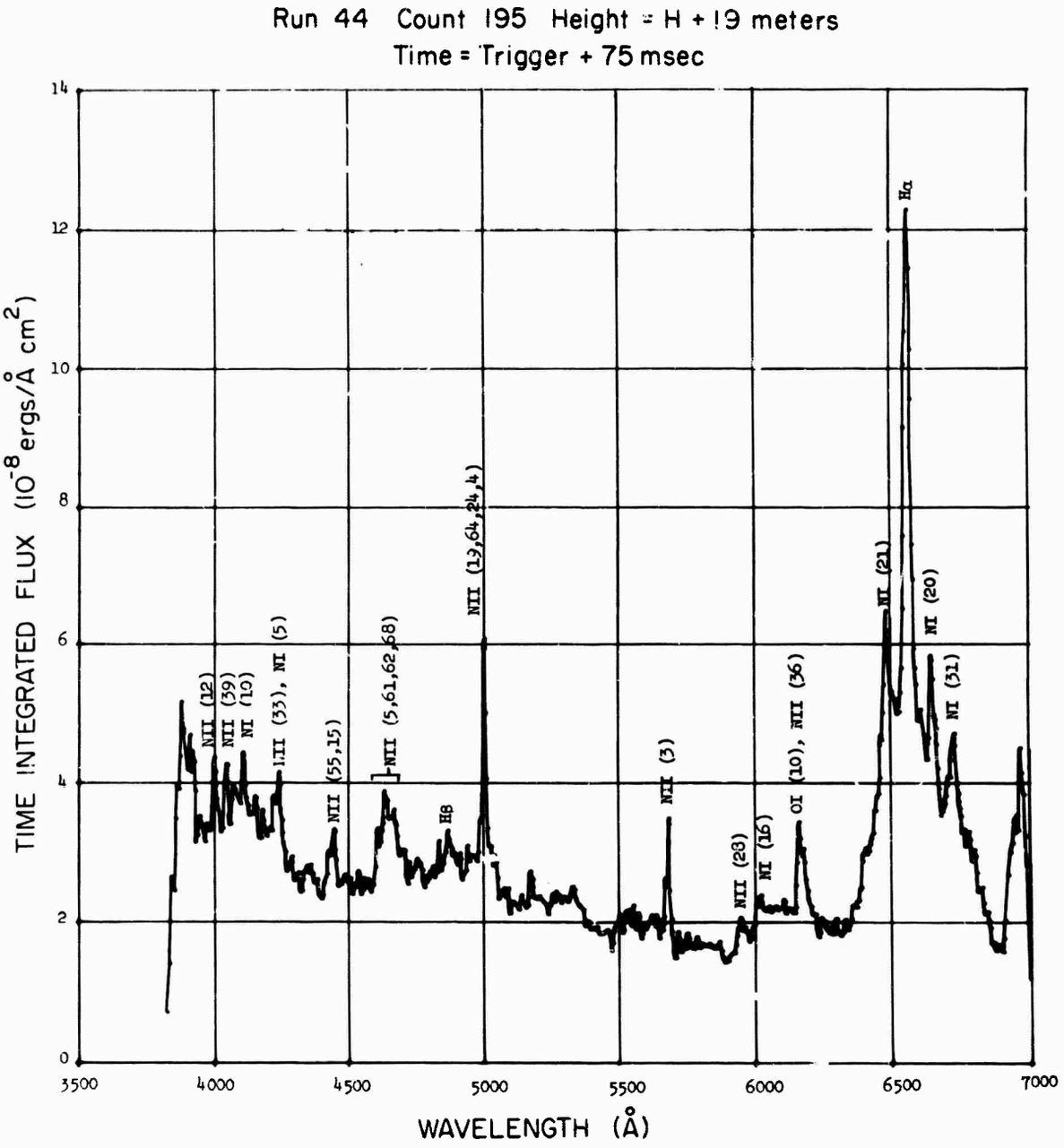

Fig. 24. Spectrum (taken at night) of probable first return stroke. Electrical energy deposited and rain transmission are unknown. Spectrum corresponds to an element of the channel at altitude H + 19 meters. Visible energy radiated = 1.2×10^{1} joule/meter, not corrected for rain transmission. Range = 12 km. Estimated rain transmission ~ 1.7×10^{-1} (refer to Fig. 23 caption).

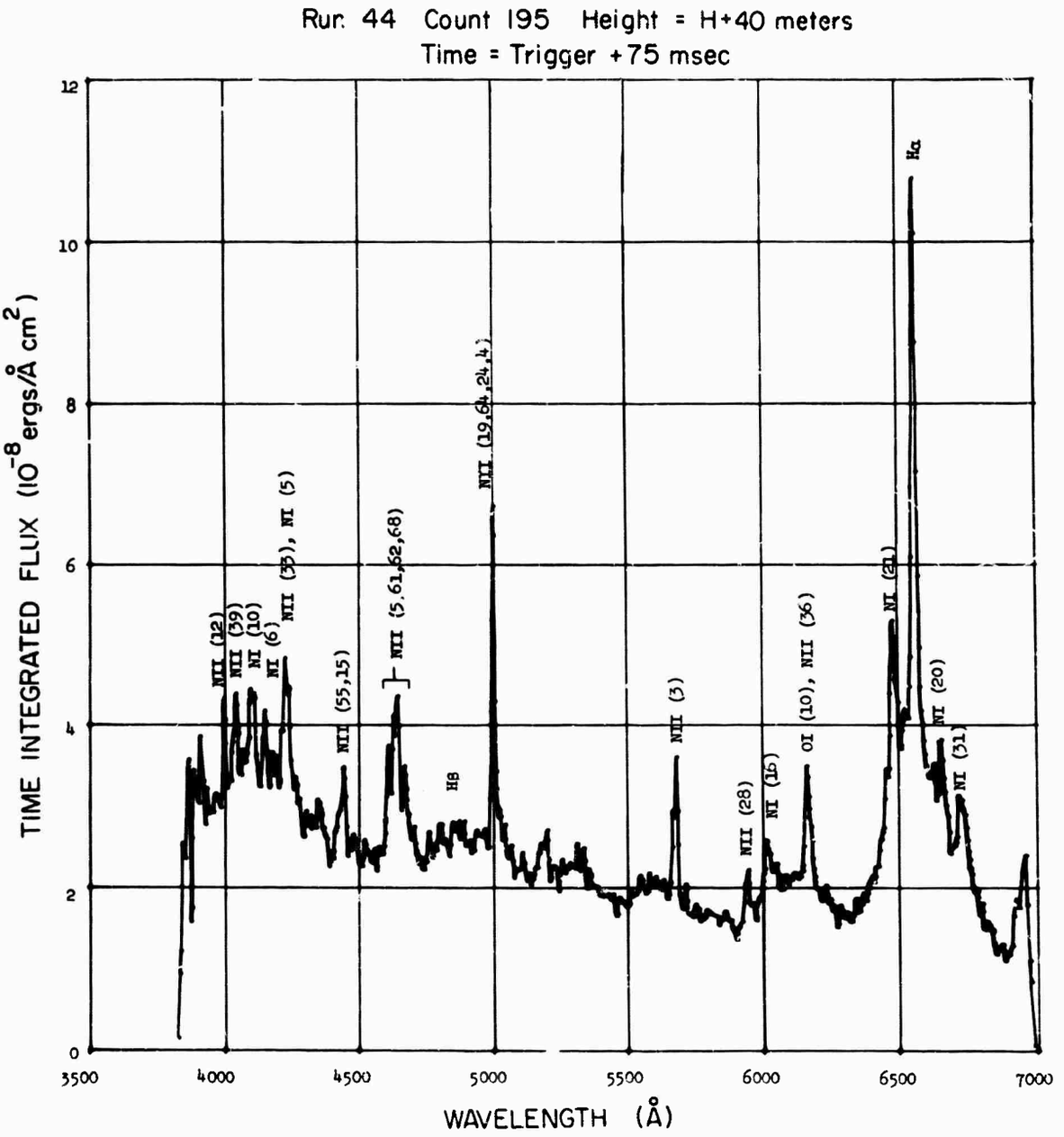

Fig. 25. Spectrum (taken at night) of probable first return stroke. Electrical energy deposited and rain transmission are unknown. Spectrum corresponds to an element of the channel at altitude H + 40 meters. Visible energy radiated = 1.1×10^4 joule/meter, not corrected for rain transmission. Range = 12 km. Estimated rain transmission is $\sim 1.7 \times 10^{-1}$ (refer to Fig. 23 caption).

1. First return strokes - The strong line features are attributable to the species NI, NII, OI, HI, and there are no molecular bandheads. If the spectrum were viewed by a 20- to 30-Å-bandwidth detector, the strongest feature, on the average, would be the blend of four NII multiplets at 5000 Å. (A feature such as NII (12) at 3995 A may have a higher peak, as seen by the spectrograph, but it is much narrower.) There is also a high density of weaker multiplets between 4000 and 4250 Å, and an Hα feature appears which, on the average, is moderately strong. Using the ratio of NII to NI radiation as a measure, the degree of ionization is higher in first return strokes than in either subsequent return strokes or continuing luminosities. The best estimate of a straight-line fit to the continuum shows that the ratio of the continuum at 3900 Å to that at 6900 Å is ~ 2.

2. Subsequent return strokes - Strong line features are attributable to the species NI, NII, OI, and HI, and there are no molecular bandheads. If the spectrum is viewed by a 20- to 30-Å bandwidth detector, the strongest feature is, in every case, Hα at 6563 Å. The next strongest is NII at 5000 Å, but it is not, on the average, much stronger than a few of the multiplets which make up a blend of features between 4000 and 4250 Å. The degree of ionization is lower than in first return strokes and higher than in continuing luminosities. The best estimate of a straight-line fit to the continuum shows that the ratio of the continuum at 3900 Å to that at 6900 Å is ~ 1.6.

3. Continuing luminosities - The major line features are attributable to NI, OI, and HI, with very weak NII. The strongest line feature in every case is Hα. The degree of ionization is lower than for return strokes. The best estimate of a straight-line fit to the continuum gives a ratio of continuum at 3900 Å to that at 6900 Å of ~ 1. There is a very much stronger, very broad blend of features between 3800 and 3900 Å. Upon rechecking original calibrations, reducing additional calibration data, and checking the magnitude of possible errors incurred in subtraction of daylight background, I must conclude that this blend of features is definitely real. In addition, the spectra of continuing luminosities are in qualitative agreement with those of Salanave. In Salanave's spectra, lines and bands are smeared in wavelength due to his method of recording, but he was able to conclude that "the continuing luminosity seems definitely strongest in that part of the spectrum favored by the CN and N_2^+ bands, and Hα."[9] The spectra presented here seem to show that continuing luminosities are not a major source of N_2^+ 1N seen by long exposure slit spectrographs.

As mentioned above, the calibrations are being reworked using additional data which should yield the best possible reduction. Preliminary results indicate an overall change in the spectra, such that the flux will be 20 to 30% higher in the blue, 5 to 15% higher in the green, and 0 to 10% lower in the red.

F. Discrimination

While the lightning spectra are not a large statistical sample, they do give complete wavelength coverage between 3900 and 6900 Å, and are therefore useful in determining whether or not there may be other or better discrimination channels than either 4150[10] or 6563 Å.

The merit of a discrimination channel must be based on the following parameters: (1) its spectral width and its average signal relative to that of the 3914-Å detection channel, (2) the sensitivity of the photodetector at the wavelength of the discrimination channel relative to that at 3914 Å, (3) atmospheric transmission at the wavelengths for detection and discrimination, and (4) the field of view and related considerations of the path by which light propagates into the detector, which can cause changes in the relative spectrum detected.

A quantitative discussion of these parameters for a discrimination channel will be presented in Volume 4. However, it is worth pointing out that a 20-Å-wide discrimination channel centered on a blend of NII multiplets near 5000 Å may be as good or better a discriminant, under a variety of storm and background light conditions, than one at either 4150 or 6563 Å.

It seems worthwhile to investigate the possibility of using a narrow band, 5000-Å channel. Toward this end the large statistical sample of

Table II. Field Change Calculations

Count No.	Stroke Time after Trigger (msec)	Scope Signal* (V)	Antenna plus Preamp Sensitivity (V^{-1})	Field Change, ΔE (V/m)	Charge Center Height (km)	Range (km)	Charge Transferred, ΔQ (C)
40.61							
	180	0.106 ± 29%	2.5×10^3	260 ± 29%	1.4 ± 20%	11.8	2 ± 60%
	235	0.138 ± 22%		340 ± 22%			3 ± 40%
	298	0.131 ± 23%		330 ± 23%			3 ± 40%
40.87							
		0.15 ± 20%	2.5×10^3	370 ± 20%	1.2 ± 20%	10.0	17 ± 40%
	75	0.15 ± 20%		370 ± 20%			17 ± 40%
	145	0.076 ± 40%		190 ± 40%			9 ± 60%
	206	0.073 ± 40%		180 ± 40%			8 ± 60%
	274	0.050 ± 62%		130 ± 62%			6 ± 80%
40.103							
		0.33 ± 50%	2.5×10^3	830 ± 50%	1.9 ± 20%*	7**	9 ± 70%
	49	0.30 ± 10%		750 ± 50%			8 ± 30%
	150	0.038 ± 100%		95 ± 100%			1 ± 100%
	188	0.42 ± 3%		1050 ± 8%			12 ± 30%
40.127							
	16	0.088 ± 35%	2.5×10^3	220 ± 35%	1.6 ± 20%	7.1	3 ± 60%
	30	0.12 ± 26%		300 ± 26%			4 ± 50%
	74	0.19 ± 21%		480 ± 21%			6 ± 40%
	147	0.053 ± 56%		130 ± 56%			2 ± 80%
40.171							
	55	0.110 ± 28%	2.5×10^4	270 ± 28%	2.3 ± 20%	4.1	7 ± 50%
40.186							
	150	0.065 ± 47%	2.5×10^4	1600 ± 47%	1.9 ± 20%	4.7	6 ± 70%

*The error corresponds to the halfwidth of the oscilloscope beam except for those signals occurring at t_o. If the signal occurred at t_o, the field strength before the stroke was unknown and the field change was estimated by comparing the Hα signal with other strokes of the same flash. The error in this case is the estimated error.

**No ranging pictures were available. After a check of available ranging data for other counts, a range of 7 km was assumed. A plot of channel length vs range from ranging picture data furthermore indicates that the vertical component of a channel at 7 km is 1.6 km. Later data on thunder indicates a range of ~ 6 km.

---

broadband (~ 200-Å) data for a channel which includes 5000 Å, taken by EG&G-operated all-sky photometers,[11] and the slit spectra obtained during the summer of 1966 will be used in the discrimination and false alarm analysis of Volume 4.

III. CALCULATION FROM ELECTRIC FIELD ANTENNA DATA OF THE CHARGE TRANSFERRED TO GROUND BY LIGHTNING

During the 1965 ARPA-AEC joint lightning study, LASL operated three electric field antennas.[7] Two of these antennas gave data on the change in the vertical component of the quasi-dc electric field caused by a lightning flash. Knowing the range and the channel length from ranging pictures and having measured the electric field change, it was then possible, on the basis of a dipole model, to calculate the charge transferred to the ground. The dipole is formed by a negative charge center near the bottom of the cloud and its image charge in the ground. It is the destruction of this dipole during a lightning stroke which produces the measured field change. The charge transferred, ΔQ, is then given by the following expression which is equivalent to that given by Malan.[12]

$$\Delta Q = 2\pi\epsilon_o \left[\frac{h^2 + R^2}{\sin \arctan\left(\frac{h}{R}\right)} \right] \Delta E$$

$$= 5.55 \times 10^{-5} \times \frac{h^2 + R^2}{\sin \arctan\left(\frac{h}{R}\right)} \times \Delta E \ ,$$

where h is the height of the charge center above

ground in kilometers, R is the distance from the stroke to the antenna in kilometers, ΔE is the vertical field change in volts per meter, and ΔQ is in coulombs. The value of h was obtained by measuring the vertical component of the length of the visible channel between ground and the cloud and assuming that the charge center was 20% higher, inside the cloud.

The "slow antenna"[13] was built by Marx Brook of the New Mexico Institute of Mining and Technology, and lent to LASL for the lightning study. Its signals were recorded both on an oscilloscope, giving field changes for the various strokes in a flash, and on paper chart, giving the total field change for a flash. The A2 antenna was a wire suspended about a meter above the ground which was kept at the same potential as the surrounding air by means of a radioactive source hung near its center, as described by Schonland.[14] The signal from this antenna was recorded on paper chart only and gave total field change for a flash.

Table II contains the results of the calculation for field changes measured from the "slow antenna" scope records.

The total field changes and total charge transferred in a flash are shown in Table III.

Table III. Total Field Change and Charge Transferred During Flash

	A2 Antenna Chart Data		Slow Antenna Chart Data		Slow Antenna Scope Data	
Count No.	ΔE (V/m)	ΔQ (C)	ΔE (V/m)	ΔQ (C)	ΔE (V/m)	ΔQ (C)
40.61	1400	13	1400	13	930	8
40.87	1700	80	1420	67	1120	57
40.103	4500	50	3300	36	2730	30
40.127	3600	47	2500	33	1130	15
40.171	6000	16	1850	5	2700	7
40.186	1700	7	3840	15	1600	6
Average		36		28		21

On the basis of the estimated errors from Table II, and the scatter in the results in Table III, the uncertainty in the calculation of the charge transferred may be about a factor of two.

The average charge transferred per stroke for 18 strokes given in Table II is 7 coulombs/stroke. This agrees with the value of 5 coulombs quoted by Malan[12] as the average charge dissipated to ground by the first stroke of a lightning flash. Malan also gives 20 coulombs as the average charge transferred to ground per flash, which is in good agreement with the 28-coulomb average for six flashes given in Table III.

The value of charge transferred in a given return stroke is used in the next section to calculate the energy deposited in the channel.

IV. EFFICIENCY OF CONVERSION OF ELECTRICAL ENERGY INTO VISIBLE RADIATION IN A LIGHTNING CHANNEL

For the spectra presented in Section II D, the energy radiated in the visible wavelength interval $3900\ \text{Å} \leq \lambda \leq 6900\ \text{Å}$ per meter of vertical component of the channel has been calculated. Each plot of the time-integrated spectral irradiance (joules/cm^2 Å) vs wavelength at the spectrograph's entrance pupil was integrated over the wavelength range throughout which the spectrograph calibrations were known accurately. The wavelength- and time-integrated irradiance, H, thus calculated was used with the range, R, and channel height, h, measured by photographic triangulation,[7] to calculate the energy per meter radiated by the channel:

$$w = 4\pi R^2 H\, h^{-1} \text{ joules/meter} .$$

Table IV contains the results of the energy calculations. Corrections have been made for atmospheric selective transmission. No correction for extinction by rain between source and detector has been included. Using the results of charge-transfer calculations made for these strokes, and range and height information from the triangulation photographs, the energy deposited per meter has been calculated.

The potential, V, of an elemental charge, q, relative to a conducting plane at a distance, h, is

$$V = \frac{1}{4\pi\varepsilon_0}\,\frac{q}{2h} .$$

The energy, W, required to assemble a charge, Q, at

Table IV. Calculation of Visible Energy

Count No.	Stroke Time after Trigger (msec)	Range (km)	Length of Channel Element** (meters)	Altitude of Channel Element (meters)	Visible Energy joules meter
40.87	87	10.0	11		17.4
40.103	-50	7.0	7.8		27.6
	0				20.3
	31				1.53
	49				15.2
	191				20.6
40.127	74	7.2	8.0		7.5
40.171	59	4.0	4.4		24.8
	71*				1.08
	77*				0.87
	83*				0.47
	89*				0.49
40.186	152	4.6	5.1		8.75
	158*				2.77
44.195	75	12.0	13.3	H***	19.0
				H + 19	11.7
				H + 40	10.6

*In the case of count 40.186, the stroke at 152 msec resulted in a time-streaked spectrum due to a continuously luminous channel; thus, while there was no "stroke" 150 msec after the trigger, this number indicates the center of the time interval over which the flux was time integrated. A similar situation exists for count 40.171 at times 71, 77, 83, and 89 msec after the trigger.

**The part of the channel imaged within the densitometer slit, i.e., the vertical length of channel over which the spectrum energy was integrated.

***In the case of count 44.195 the spectrum was high enough to permit three different densitometer scans.

---

a distance, h, from the ground is then

$$W = \int_0^Q V\,dq = \frac{1}{4\pi\epsilon_0}\int_0^Q \frac{q}{2h}\,dq = \frac{1}{4\pi\epsilon_0}\,\frac{Q^2}{4h}\,.$$

Assuming that this energy is dissipated in a lightning channel by the transfer of charge to ground, the energy deposited per meter is

$$w = \frac{1}{4\pi\epsilon_0}\,\frac{Q^2}{4h^2} = 2.25 \times 10^9 \left[\frac{Q(\text{coul})}{h(\text{meter})}\right]^2 \frac{\text{joule}}{\text{meter}}\,.$$

Using these values of deposited energy and measured values of visible energy radiated, the efficiency, ϵ, for conversion of electrical energy to visible radiation can be calculated. However, the values of visible energy given in Table IV must first be corrected for transmission through rain.

Transmission through rain is discussed in the Appendix. To determine the rain extinction coefficient, it was first assumed that it was raining all along the path to the stroke at a rate of 10 mm/hour which corresponds to a typical Los Alamos rainfall. This rate corresponds to an extinction coefficient of $\sim 0.86\ \text{km}^{-1}$. Assuming values ranging from 0.0 through 2.0 for the extinction coefficient, it was possible to calculate an efficiency for seven strokes. The largest errors in the efficiencies are due to uncertainties in the rain transmission correction. These uncertainties are smallest for the closest strokes and proportional to the rain transmission correction. Therefore, a weighted average of the efficiency is taken in which the rain transmission, T_r, is the weighting factor. The weighted average is then

$$\bar{\epsilon} = \frac{\Sigma \epsilon T_r}{\Sigma T_r}\,.$$

For each value of extinction coefficient assumed, an average deviation was calculated, and the plot of mean deviation vs extinction coefficient is shown in Fig. 26. It is seen that there is a minimum mean deviation for an extinction coefficient of $0.475\ \text{km}^{-1}$. This figure was selected as the best estimate of the rain extinction coefficient and corresponds to an average rainfall of approximately 5 mm/hour.

The results of the various calculations are listed in Table V.

In summary, the visible energy radiated (3900 to 6900 Å) per unit of length of lightning channel has been calculated using time- and wavelength-integrated spectrographic data of the 1965 lightning study. An estimated rain-transmission correction was used. The total energy deposition was calculated, assuming a dipole model of a lightning stroke and using measured values of charge transferred and channel length. The efficiency for conversion of electrical energy to visible radiation is found to be 0.007 ± 36%.

Table V. Calculation of Efficiency

Count No.	Stroke Time after Trigger (msec)	Range (km)	Rain Transmission	Visible Energy* (joules/meter)	Energy Deposited (joules/meter)	Efficiency (ε)
87	87	10.0	8.7×10^{-3}	2.0×10^{3}	3.3×10^{5}	6.1×10^{-3}
103	0	7.0	3.6×10^{-2}	5.6×10^{2}	5.1×10^{4}	1.1×10^{-2}
103	49	7.0	3.6×10^{-2}	4.2×10^{2}	4.0×10^{4}	1.1×10^{-2}
103	191	7.0	3.6×10^{-2}	5.7×10^{2}	9.0×10^{4}	6.4×10^{-3}
127	74	7.2	3.3×10^{-2}	2.3×10^{2}	3.2×10^{4}	7.3×10^{-3}
171	59	4.6	1.1×10^{-1}	2.2×10^{2}	2.1×10^{4}	1.1×10^{-2}
186	152	4.0	1.5×10^{-1}	5.9×10^{1}	2.2×10^{4}	2.6×10^{-3}

Extinction Coefficient Due to Rainfall = $0.475\ km^{-1}$.

Weighted Average Efficiency = $0.007 \pm 36\%$.

*Corrected for (1) humid-air transmission and (2) estimated rainfall transmission.

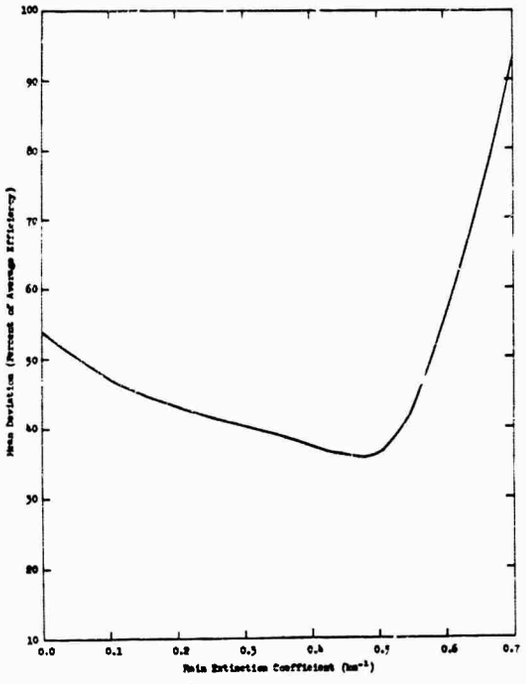

Fig. 26. Plot of mean deviation of efficiency vs rain extinction coefficient. The best estimate of rain extinction coefficient for run 40 was chosen as that which minimized the mean deviation.

APPENDIX

ATMOSPHERIC TRANSMISSION

1. The transmission of dry air is given by

$$T_a = \exp\left[-\mu_a(\lambda)\,\frac{R}{8.01}\,\frac{P}{760}\,\frac{273}{T}\right],$$

where $\mu_a(\lambda)$ is the wavelength-dependent extinction coefficient for molecular scattering, given by Allen;[15] R is the range of the lightning stroke in kilometers; P is the partial pressure of air in Torr; and T is the temperature in degrees K.

2. The transmission of water vapor is given by

$$T_{wv} = \exp\left[-28.86\,\mu_{wv}(\lambda)\,(R.H.)\,R\,\frac{E}{T}\right],$$

where $\mu_{wv}(\lambda)$ is the wavelength-dependent extinction coefficient for water vapor, given by Allen;[15] R.H. is the relative humidity expressed as a decimal fraction; R is the range of the stroke in kilometers; and E is the saturated water vapor pressure in Torr at temperature T in degrees K.

The transmission of humid air is the product of T_a and T_{wv}.

3. Transmission through rain whose drop diameter is larger than 10 μ is wavelength-independent in the visible, according to Middleton.[16] The extinction coefficient for water drops is then given by[16]

$$\mu_{wd} = 2 \times 10^5 N \pi a^2 \ (km^{-1})$$

where N is the number density (cm^{-3}) of drops of radius a (cm).

Hardy[17] has published data on drop-size distributions for various rates of rainfall at Flagstaff, Arizona. A rough numerical integration of extinction coefficient over drop size distribution was carried out, and the resultant extinction coefficient is plotted as a function of rain intensity in Fig. 27.

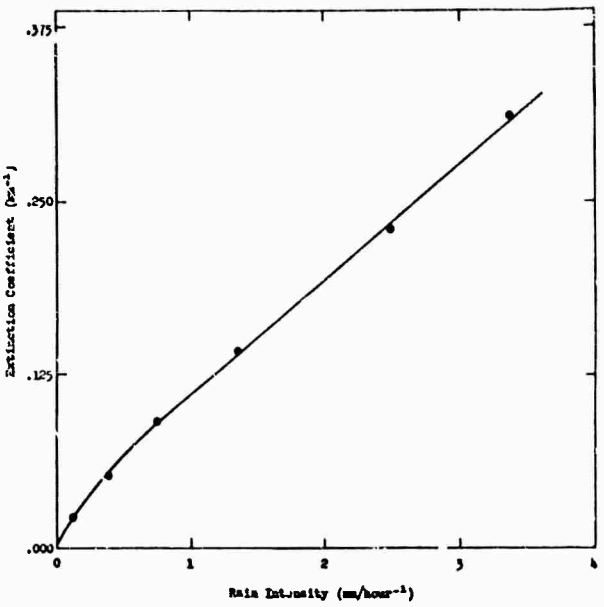

Fig. 27. Extinction coefficient for raindrops vs rain intensity as calculated by means of a rough numerical integration over raindrop size distribution published by Hardy.

ACKNOWLEDGMENTS

The program was carried out under the direction of Herman Hoerlin, and I thank him for the opportunity to participate, and for his encouragement and suggestions. I also thank G. E. Barasch, K. B. Mitchell, H. M. Peek, and S. N. Stone without whose discussions, and help with spectrographic technique, my efforts would have been much less successful. Thanks are also due L. M. Duncan for her effort in densitometry and the running of computer programs, to D. L. Stam for illustrations, to S. F. Waber for reducing the photographic ranging data, and to Barbara Anderson for her secretarial work.

This program is part of a DOD-ARPA and AEC-sponsored effort to improve ground-based nuclear test detection capabilities. Thanks are also due Lt. Col. John Hill and other personnel of the Nuclear Test Detection Division of ARPA for their active interest in the problems.

REFERENCES

1. L. E. Salanave, Science 134, 1395 (1961).
2. P. Fox, Astrophys. J. 18, 294 (1903).
3. F. Israel and K. Wurm, Naturvissenschaften 29, Heft 52 26.12, 778 (1941).
4. A. B. Meinel and L. E. Salanave, J. Atmos. Sci. 21, 157 (1964).
5. F. D. Harrington, "An f/2.8 Low-Dispersion Time-Resolving Grating Spectrograph," NRL 5576, Feb. 7, 1961.
6. C. E. Moore, NBS Tech. Note No. 36, Nov. 1959.
7. G. E. Barasch, "Lightning Study in Los Alamos - Weather and Coordination Data," LASL internal document, July 1, 1965.
8. ARPA Quarterly Report, April 1 - June 30, 1966, LASL internal document, August 5, 1966.
9. L. E. Salanave, "The Photographic Spectrum of Lightning; Determination of Channel Temperature from Slitless Spectra," Problems of Atmospheric and Space Electricity, S. C. Coroniti, Ed., Elsevier Publishing Co., New York, 1965.
10. D. R. Vestervelt and H. Hoerlin, Proc. IEEE 53, 2067 (1965).
11. R. A. Amato, "Spectral and Temporal Characteristics of Lightning as Measured with Wide-Angle Detector," Vol. I, WG&G Tech. Report B-3506, March 1967.
12. D. J. Malan, Physics of Lightning, English Universities' Press, Ltd., London, 1963.
13. N. Kitagawa and M. Brook, J. Geophys. Res. 65, 1189 (1960).
14. B. F. Schonland, Atmospheric Electricity, John Wiley & Sons, Inc., New York, 1953.
15. C. W. Allen, Astrophysical Quantities, Oxford Univ. Press, 1963, p. 122.
16. W. E. K. Middleton, Vision Through the Atmosphere, Univ. Toronto Press, 1958, p. 29.
17. K. R. Hardy, J. Atmos. Sci. 20, 299 (1963).